Authors’ response

We thank the referees for their comments and questions that have helped us improve the manuscript.
We have:

- clarified the Jakobshavn example,
- compared our results with Mercenier et.al (2018) in the introduction as well as the discussion,
- discussed under what conditions the derived cliff calving relation is valid (sliding, lateral drag) and
- extended the discussion of time to failure with a focus on uncertainties.

Following, we give detailed replies to the referees’ comments.

Anonymous Referee #1

Major comments

The model used to derive the proposed analytical calving law has a highly simplified geometry – with zero surface or bed slope, no lateral drag, and no sliding at the bed. Previous studies have shown that the extent of the “failure region” discussed in this paper is strongly affected by basal sliding rates (Ma et al., 2017). Likewise, other studies have shown that the stress regime around the calving front is strongly affected by surface slope (Mercenier et al, 2018).
As the authors point out, “there are no glaciers currently available where cliff calving is the primary failure mechanism”, but modelling studies such as DeConto and Pollard (2016) suggest cliff failure could occur in future in deep Antarctic basins, after rapidretreat of their buttressing ice shelves. These environments are highly likely to experience basal sliding, as well as lateral drag. It is hard to say what proportion of ice cliffs might meet the authors’ conditions, but the proposed model for predicting calving rates seems a lot less generally applicable than simply using the maximum shear stress to define a new calving front location. At the very least the paper should include
more discussion of precisely what circumstances the model is valid for, and under what conditions (e.g. basal sliding) it is likely to fail.

Response: We thank the reviewer for this valuable suggestion. We gave a lengthy reply to the effect of sliding and lateral drag in the short comment answering this review and have included a discussion in the manuscript (section 7.1)

Minor comments

Page 2 line 6: Columbia glacier is in Alaska, not Canada
Response: Thank you, this has been corrected.

Page 2 lines 28-29: The description of Mercenier et al. (2018) is extremely brief and doesn’t contrast the model with other studies, which would be much more informative. This also seems a suitable point to reference Morlighem et al. (2016).
Response: Done (p.2, l.27; p.2, l.33 – p.3. , l.2). A more in depth discussion of Mercenier is given in the discussion (section 7.3.2)

Introduction: The introduction misses damage mechanics methods which have been used to implement calving in a tidewater glacier (Krug et al., 2014).
Response: Done (p.2, l.25-27).

Page 3 line 5: “it is not clear what a cliff calving law would look like”. Are the authors aware of Bassis et al. (2017) which already implemented a calving law based on cliff instability?

Response: Thank you for pointing this out, the reference has been included (p.3, l.5).

Page 4 lines 5-10: No boundary condition is provided for the upstream boundary of the model (r.h.s. in figure 1)
Response: The upstream boundary condition has been added. No inflow is assumed at this boundary.

Page 5, eq. 11: Should y in this equation be z?
Response: Yes, it has been corrected.

Page 7 lines 2-3: "However, it does not take into account whether deviatoric stresses are tensile or compressive or shear stresses and this is likely to be important for ice failure." Surely this is the advantage of using the von Mises stress as a criterion – it is able to allow for failure under both tension and shear, and is therefore more widely applicable than a criterion that considers only one mechanism of failure?
Response: The reviewer makes a valuable point. However, the maximum shear stress and the von Mises stress differ only by a factor of √3. Choosing the von Mises stress instead of the maximum shear stress as the failure criterion would not change the results qualitativley. We chose the shear stress because it gives a more clear physical explanation of how the failure happens. This discussion has been added to the manuscript (p.6, l.9-10; l.25-26).

Page 7 lines 5-10: these uncertainties should be explored further in the discussion, which doesn't currently make their magnitude clear.
Response: Estimate of the magnitude has been given (p.7, l.1 and section 7.2).

Page 7 eq. 13: I'm not sure where the term sqrt(μˆ2+1) on the l.h.s. comes from here.
Response: Me neither, the derivation is not given in the cited literature. Eq. 12 expresses the failure condition in terms of the stresses along the future fault plane and therefore depends on the direction of the fault plane. Eq. 13 gives a more general expression of the failure condition in terms of the maximum shear stress and the isotropic pressure. This has been clarified in the manuscript (p.8, l.1).

Page 9 line 1: "Above a critical freeboard of about 1000m the failure region encompasses the whole ice thickness." Is this based on results from figure 4?
Response: Yes. This has been added in the manuscript (p.8, l.23).

Page 9 lines 3-4: "The freeobard [sic]- failure region relation has a bend at the critical freeboard and hence the two parts require separate analytical fits" Figure 5 shows no freeboards above 800 m, so readers cannot see how this conclusion was reached.
Response: The figure has been modified to show larger freeboards.

Page 10 eq. 18: What are k, r and B?
Response: k, r and B are material constants. This has been added in the manuscript (p.10, l.9).

Page 11 eq. 19 & 20: I think σ and σ0 here are not the same as in previous equations?
Response: No, they are not. σ is the major stress and σ0 is the instantaneous strength. This has been added in the manuscript (p.12, l.5).

Page 11 eq. 21: Is part of this equation missing? What values have you used for k, D0 and Dc?
Response: All the material properties have been included in B, which has been renamed B* to avoid confusion.

Page 13 bullet point 3: This sentence does not make sense, please rephrase.
Response: Done.

Page 13, figure7: I don't think this figure is referenced in the text?
Response: Done.

Page 14 line 4: "Where the failure region does not encompass the whole ice thickness, an analytical fit was made." This sentence is quite unclear. To my understanding, your results use an analytical fit which is only valid for freeboards less than 1000 m? Is that what was meant here?

Response: Yes, this was clarified (p.15, l.7).

Page 14, line 6: The authors conclude that the application to Jakobshavn glacier demonstrates that the modelled calving rate can be "realistic". I'm not sure that theresults support a strong conclusion here. The modelled calving rate is lower than the observed calving rate, which is appropriate. But the modelled calving rate could increase by a factor of ten and still meet this condition. I think the discussion needs to be a lot more clear about the very large uncertainties in calving rates produced by this model.

Response: We use Jakobshavn to show that cliff calving rates are not overestimated (p.13, l.3-5). A discussion about the uncertainties has been included (section 7.2).

There are also quite a number of spelling and grammar mistakes in the document, and I suggest additional proof reading before resubmission.

Response: Spelling and grammar have been checked.

Anonymous Referee #2

Major comments

To derive the calving relation, the authors compute the stresses in the vicinity of synthetic ice fronts with various thicknesses and water depth using a full-Stokes ice flow model. A stress criteria (based on the maximal shear stress) is used to define the region that will calve. This is further converted to a calving rate using a reference failure time. As pointed by Vieli and co-authors, this study is extremely similar to Mercenier et al. (2018), and do not really acknowledge it. As Schlemm and Levermann re-use the failure time calibrated by Mercenier et al. (2018), the only difference is the stress criteria and thus the failure region. The first reviewer and Vieli and co-authors, already provide guidance to improve the paper by clarifying the hypotheses, running more sensitivity experiments, comparing with previous similar studies and improving the discussion to define the applicability of the proposed calving law. I fully support their main comments and this implies major changes in paper.

Response: The section about the time to failure has been expanded to clarify that the time to failure Mercenier et al. (2018) derived for tensile failure might not be suitable to shear failure, but is used nevertheless because there are no better guesses available. The discussion section has been expanded significantly to include discusion about the effect of sliding and lateral drag on the cliff calving rate (section 7.1), uncertainties in the time to failure (section 7.2), as well as a comparison with other cliff calving parametrisations and with the study of Mercenier et al. (2018) (section 7.3).

Finally, at the end, Jackobsahvn is presented as one of the few glaciers that is "in the calving cliff regime" ; However, this "cliff regime" is not really defined, from page 7 lines 29-30, I understand that the authors define the cliff regime from their critical shear stress; So a glacier would be in the cliff regime if their critical shear stress is reached somewhere in the domain; which from their numerical experiments appends only for freeboards larger than 100m? At the end it is a bit disappointing that the proposed parameterisation underestimate the calving rate of one the few glaciers in what the authors call the "calving cliff regime", by more than one order of magnitude. Especially when the parametrisation from Mercenier et al. (2018) does a fairly good job for the same glacier.

Response: A glacier enters the cliff calving regime, when its freeboard is larger than the critical freeboard Fc and the cliff calving rate given by eq. 22 becomes nonzero. This definition has been added to the text (p.13, l.3) and the discussion has been extended to clarify that we expect cliff calving (i.e. shear failure) to play a role in Jakobshavn but since the freeboard is still rather small and the glacier is heavly crevassed, we expect tensile failure to be the main contribution to the overall calving rate. The Jakobshavn example is meant to be a "sanity check" and can only give an upper bound on the cliff calving rate.

As shown by Vieli, the Schlemm and Levermann caving rates become higher than the Mercenier et al. calving rates for larger free boards. So the paper should really focus on giving better description and justification for their mechanism, and its domain of applicability. Should it replace existing parameterisations for large freeboards? In this case how to define the transition to the cliff regime? Should we sum the processes or take the maximum calving rate? Without answering theses question properly I don't see how the proposed parametrisation could be used by the community.

Response: Unfortunately, we cannot give a definite answer to these questions. We expect tensile failure to dominate for small freeboards and shear failure to dominate for large freeboards. However, it is difficult to say at which glacier freeboard the tensile failure regime ends and the shear failure regime begins, not only due to uncertainty in the scaling parameter C0. In practice, both failure modes will interact, with tensile stress damaging the ice through few large crevasses originating from the surface of the ice and shear stress damaging the ice through a large number of small fractures in the lower part of the cliff. This likely interaction of failure modes cannot be analyzed by assuming ice to be a continuous medium (like the approach used here and by Mercenier et al. (2018)), but should be done with damage theory or a discrete element approach. This is discussed in section 7.3

Minor comments

Abstract: the mechanism "cliff-calving" is not really defined in the abstract and there is a confusion with "normal" calving of tide water glaciers as currently observed, see comment above. This distinction and the definition of "cliff calving" is also not really clear in the introduction. It should be clear since the beginning that the paper propose an extension (extrapolation) of the calving mechanism to glacier freeboard heights that are not currently observed.

Response: This was clarified in the abstract.

Page 1, lines 18-22: the word "loss" introduces a confusion between the processes that remove ice from the ice sheets (what is implied with the reference to Antarctica), and the fact that the ice sheets are not in balance due to increase losses by calving and/or melt (the numbers for Greenland are the respective contribution to the unbalance). Please clarify.

Response: This has been clarified.

"Failure region" everywhere in the text and Figures 3-4-5. There is a confusion between the region where the stress is higher than the threshold and the "failure distance" L. It seems that L is the maximum distance from the front where the stress is in excess to the critical stress. Please clarify.

Response: This was clarified (section 4)

Figure 4. What is the color scale? Indicate that the outline for H=1000m is also shown in Fig. 3 (top-left).

Response: An explanation of the color scale and mention of the outline has been added to the figure caption.

Page 9, line 4: clarify the "bend" and the "two fits" at the critical freeboard.

Response: Done (p.8, l.25-27).

Page 9, Eqs. 14-17: explain the values for the fit; which ones have been optimised, which ones are prescribed and why?

Response: At first L was fitted as a function of F for each value of w. Then the parameter functions Fs,Fc and s were fitted as functions of w. This has been added to the manuscript (p.10, l.1-2).

Page 11: comparison with Jackobsahvn; clarify the discussion about the grounding line and front.

Response: Done (p.13, l. 6-10).

A simple stress-based cliff-calving law

Tanja Schlemm[1,2] and Anders Levermann[1,2,3]

[1]Potsdam Institute for Climate Impact Research, Potsdam, Germany
[2]Institute of Physics and Astronomy, University of Potsdam, Potsdam, Germany
[3]Lamont-Doherty Earth Observatory, Columbia University, New York, USA

Correspondence: Anders Levermann (anders.levermann@pik-potsdam.de)

Abstract. Over large coastal regions in Greenland and Antarctica the ice sheet calves directly into the ocean. In contrast to ice-shelf calving, an increase in [..[1]]calving from grounded glaciers contributes directly to sea-level rise[..[2]]. Ice cliffs with a glacier freeboard larger than ≈ 100 m are currently not observed, but it has been shown that such ice cliffs are increasingly unstable with increasing ice thickness. This cliff calving can constitute a self-amplifying ice loss mechanism that may significantly alter sea-level projections both of Greenland and Antarctica. Here we seek to derive a [..[3]]minimalist stress-based [..[4]]parametrization for cliff calving [..[5]]from grounded glaciers whose freeboards exceed the 100 m stability limit derived in previous studies. This will be an extension of existing calving laws for tidewater glaciers to higher ice cliffs.

To this end we compute the stress field for a glacier with a simplified two-dimensional geometry from the two-dimensional Stokes equation. First we assume a constant yield stress to derive the failure region at the glacier front from the stress field within the [..[6]]glacier. Secondly, we assume a constant response time of ice failure due to exceedance of the yield stress. With this strongly constraining but very simple set of assumption we propose a cliff-calving law where the calving rate follows a power-law dependence on the freeboard of the ice with exponents between 2 and 3 depending on the relative water depth at the calving front. The critical freeboard below which the ice front is stable decreases with increasing relative water depth of the calving front. For a dry water front it is, for example, [..[7]]75 m. The purpose of this study is not to provide a comprehensive calving law, but to derive a particularly simple equation with a transparent and [..[8]]minimalist set of assumptions.

[1]removed: cliff calving directly contributes
[2]removed: and a monotonously increasing calving rate with ice thickeness
[3]removed: minimalistic
[4]removed: parameterization
[5]removed: .
[6]removed: ice sheet
[7]removed: 75m
[8]removed: minimalistic

1 Introduction

Ice loss from Greenland and Antarctica is increasingly contributing to global sea-level rise (Rignot et al., 2014; Shepherd et al., 2018; WCRP Global Sea Level Budget Group, 2018). A possible additional future mass loss from these ice sheets is of crucial importance for future sea-level projections (Slangen et al., 2017; Church et al., 2013; DeConto and Pollard, 2016; Kopp et al., 2017; Mengel et al., 2016; Ritz et al., 2015; Levermann et al., 2014). Ice sheet gain mass by the surface mass balance. The question whether they contribute to changes in sea level is determined by the question how strongly this mass addition is compensated or overcompensated by mass loss. Both ice sheet in Greenland and Antarctica currently show a net ice loss. Calving accounts for roughly half the ice loss of the Antarctic ice shelves, the rest is lost by basal melt (Depoorter et al., 2013). For the Greenland ice sheet, calving accounted for two-thirds of the ice loss between 2000 and 2005, the rest is due to enhanced surface melting and runoff (Rignot and Kanagaratnam, 2006). Because surface melt increased faster than glacier speed, calving accounted for one-third of the Greenland ice sheet mass loss between 2009 and 2012 (Enderlin et al., 2014).

Tidewater glaciers calve vigorously when they are near floatation thickness producing icebergs with a horizontal [..[9]]extent smaller than the ice thickness. This has been expressed in semi-empirical height-above-floatation calving laws (Meier and Post, 1987; van Der Veen, 1996; Vieli et al., 2002). Calving at ice-shelf fronts or floating glacier tongues has long rest periods [..[10]]interrupted by the calving of large [..[11]]tabular ice bergs (Lazzara et al., 1999) and is preceded by the formation of deep crevasses upstream (Joughin and MacAyeal, 2005). The distinction between these two kinds of calving is not always easy because a tidal glacier can form or lose a floating tongue; this has for example been observed at the Columbia glacier in [..[12]]Alaska (Walter et al., 2010).

In order to model calving not just for single glaciers but for whole ice sheets, a calving parametrization is needed. Theories describing the nucleation and spreading of crevasses in ice (Pralong and Funk, 2005) are computationally very intense and difficult to apply in simulations on long timescales and large spatial dimensions. In order to [..[13]]parametrize calving processes several approaches have been used:

First, calving can be described as a function of strain rate and crevasse depth. Nye (1957) first described the formation of crevasses as a result of velocity gradients: The depth of the crevasse is determined by the strain-rate and overburdening pressure of the ice. Observations show that ice velocities are greater near the calving front than upstream (Meier and Post, 1987), hence crevasses form mainly at the calving front. When crevasses are deep enough[..[14]]. Icebergs are then separated from the glacier and calve off. Benn et al. (2007) proposed a calving law with the assumption that a glacier calves where crevasses reach the water level, Nick et al. (2010) proposed calving when surface and basal crevasses meet. These calving laws have been applied successfully in 1D [..[15]]flow-line models (Nick et al., 2010) and in a 3D Full Stokes model (Todd et al., 2018).

[9] removed: extend
[10] removed: interupted
[11] removed: tabulare
[12] removed: Canada
[13] removed: parameterize
[14] removed: , icebergs are
[15] removed: flowline models Nick et al. (2010)

Second, a number of approaches have been taken to analyze calving processes via the stress balance. Bassis and Walker (2011) analyzed depth-averaged stresses at the calving front. Considering tensile and shear failure, they found that there is an upper [..[16]]limit for the thickness of stable ice cliffs: an ice cliff is only stable if the glacier's freeboard (ice thickness minus water depth) is lower than 200m. The limit decreases to 100m if weakening of the ice through crevasses is also considered. [..[17]]Krug et al. (2014) used damage and fracture mechanics to model calving. This approach using linear elastic fracture mechanics has recently been analyzed by Jiménez and Duddu (2018) who found that it can be applied to floating shelves but not to grounded glaciers. Morlighem et al. (2016) give a calving rate in terms of ice velocity and the von Mises stress. Recent works by Ma et al. (2017) and Benn et al. (2017) solved the 2D full-Stokes equation at the calving front with finite element methods. Ma et al. (2017) found that while sliding glaciers calve through tensile failure, for glaciers frozen to the bed shear failure dominates. Benn et al. (2017) used finite element models to solve the stress balance and a discrete element model to [..[18]]simulate fracture formation. They modelled a range of calving mechanisms including calving driven by buoyancy and melt-undercutting, but did not give parametrizations of calving rates.

Finally, Mercenier et al. (2018) [..[19]]analyzed tensile failure with 2D finite elements and derived a calving law for tidewater glaciers. They analyzed crevasse formation at the glacier terminus, determined the distance of the crevasse to the front and the time to failure until the crevasse penetrates the whole glacier and the iceberg in front of the crevasse calves off. Together this gives an equation for the calving rate as a function of water depth and ice thickness.

All these approaches [..[20]]agree on the basic physics of glacier calving: Thicker ice at the terminus leads to higher stresses and larger calving rates. Glaciers terminating in water are stabilized by the water's back-pressure and have smaller calving rates.

The stability limit derived by Bassis and Walker (2011) lead to the formation of the marine ice cliff instability hypothesis. [..[21]]If cliff calving from ice cliffs whose freeboards exceed the stability limit [..[22]]is initiated in an overdeepend basin, e.g. in East Antarctica, it can lead to runaway cliff calving where higher ice cliffs are exposed the further the grounding line retreats, causing even larger cliff calving rates.

Pollard et al. (2015) and DeConto and Pollard (2016) incorporated cliff calving in Antarctica projections by assuming a linear relation between freeboard exceeding the stability limit and calving rate and showed that the marine ice cliff instability can lead to much faster sea level rise than [..[23]]found in previous approaches. Bassis et al. (2017) rewrote the condition that the glacier freeboard should not exceed the stability limit as a lower bound on the rate of terminus advance or equivalently an upper bound on the calving rate. More research is needed and especially a more physically based cliff calving law. Studies

[16]removed: thickness limit for
[17]removed: More recent
[18]removed: model
[19]removed: analysed
[20]removed: aggree
[21]removed: Here, cliff calving means calving
[22]removed: . If cliff calving
[23]removed: expected

by Ma et al. (2017), Benn et al. (2017) and Mercenier et al. (2018) were made for tidewater glaciers not exceeding the stability limit and [..[24]]might not be applicable to glaciers exceeding the stability limit.

In this study, we [..[25]]analyze stresses at the calving front by solving the 2D Stokes equation with a finite element model in order to propose a simple cliff calving law. The purpose of this study is not to provide a comprehensive analysis. By contrast, we [..[26]]seek a minimalistic set of assumptions that paths the way to a simple stress-based cliff calving law.

2 Stress balance near the calving front

2.1 Problem set-up: 2D Stokes equation and boundary condition

In this study we consider a plane, flat glacier of constant thickness H terminating in water of depth D in a one-dimensional ([..[27]]flow-line) model with horizontal coordinate x and vertical coordinate z (Figure 1).

In order to compute the stress field near the calving front we set the glacier to be grounded (relative water depth $w \equiv D/H < 0.9$) and frozen to the bed. The numerical domain has a length of $L = 6 \cdot H \gg H$. The factor 6 was chosen as a compromise to reduce computational effort while ensuring that the upstream boundary does not effect stresses at the glacier terminus. L could have been chosen to be truly "much larger" than H but that would have required a lot of computation time without significantly benefiting the precision of the calculation. The [..[28]]flow-line assumption is justified, for example, in situations where the glacier is wide in comparison to its length and thickness. In these cases lateral stresses can often be neglected. The flow line assumption is a strong constraint which neglects, for example, any buttressing effects within the ice sheet. However, the considered geometry with the width [..[29]]of the glacier much larger than the horizontal extent in [..[30]]the flow-line direction [..[31]]$L = 6 \cdot H$ is internally consistent and applicable to a number of situations observed both in Greenland and Antarctica. The assumption of a flat ice thickness is justifiable on a horizontal scale of several hundred meters to a few kilometers.

The ice flow and the stresses within the ice are governed by the Stokes equations,

$$\partial_x \sigma_{xx} + \partial_z \sigma_{xz} = 0, \tag{1}$$

$$\partial_x \sigma_{zx} + \partial_z \sigma_{zz} = f \tag{2}$$

and the continuity [..[32]]equation,

$$\nabla \cdot \boldsymbol{u} = \partial_x u_x + \partial_z u_z = 0 \tag{3}$$

[24] removed: it is not clear what a cliff calving law would look like
[25] removed: analyse
[26] removed: see
[27] removed: flowline
[28] removed: flowline
[29] removed: been
[30] removed: flow direction L and
[31] removed: been
[32] removed: equations

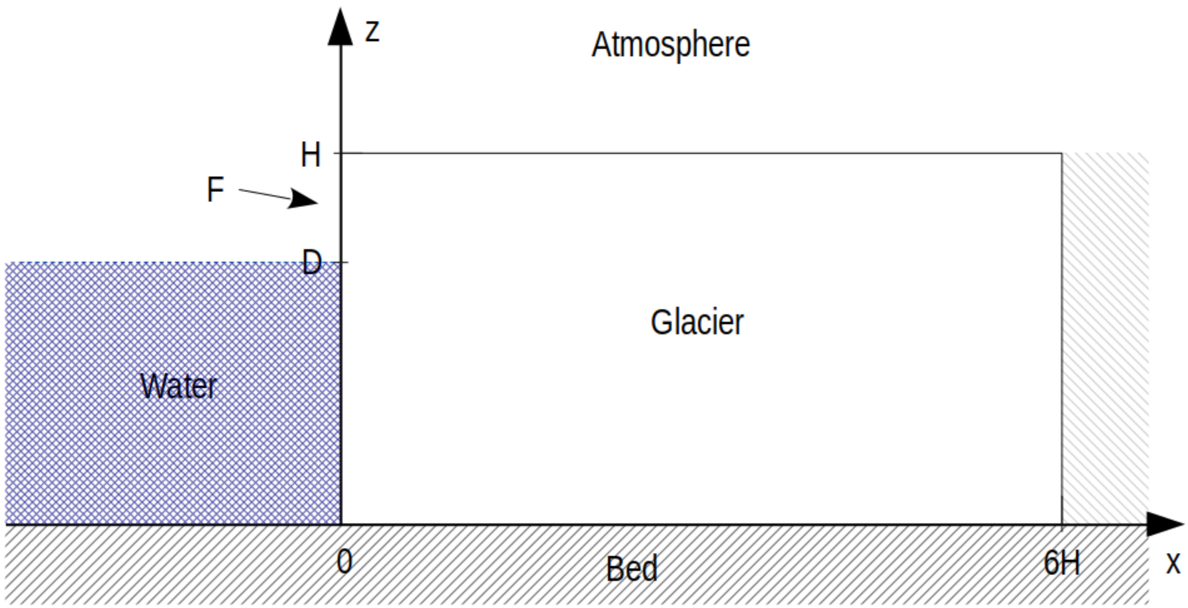

Figure 1. Geometrical set-up of the stress computation: two-dimensional plane flat glacier frozen to the bedrock with a calving front at its terminus. The glacier length L is six times as large as the glacier height H in order to ensure that the boundary condition on the right does not significantly influence the stress field at the terminus on the left. The ice thickness is denoted H, ice thickness below the water level is D and the free-board is denoted F.

with the Cauchy stress tensor σ and the gravitational force f. The Cauchy stress tensor can be split into an isotropic pressure P (also called cryostatic pressure) and the deviatoric stress tensor S, such that

$$\sigma_{ij} = -P \cdot \delta_{ij} + S_{ij} \tag{4}$$

where δ_{ij} is the Kronecker delta. Ice rheology is assumed to be given by Glen's flow law (van der Veen, 1999),

$$\dot{\epsilon}_{ij} = A S_e^{n-1} S_{ij}\,, \tag{5}$$

with the strain rate tensor $\dot{\epsilon}_{ij} = \frac{1}{2}\left(\partial_i u_j + \partial_j u_i\right)$ and the effective stress $S_e = \sqrt{\frac{1}{2}S_{xx}^2 + \frac{1}{2}S_{zz}^2 + S_{xz}^2}$.

The surface boundary is assumed to be traction-free. At the calving front boundary, we assume traction continuity to the water pressure and no traction above the water line. At the glacier bed, a no-slip boundary condition is assumed, which corresponds to a glacier frozen to its bed. No inflow is assumed at the upstream boundary.

ice top: $$\sigma \cdot \boldsymbol{n} = \begin{pmatrix} \sigma_{xz} \\ \sigma_{zz} \end{pmatrix} = \boldsymbol{0}, \tag{6}$$

ice base: $$\boldsymbol{u} = \boldsymbol{0}, \tag{7}$$

ice front: $$\sigma \cdot \boldsymbol{n} = \begin{pmatrix} -\sigma_{xx} \\ -\sigma_{xz} \end{pmatrix} = \begin{cases} (-\rho_w g z, 0), & z < D \\ (0,0), & z > D \end{cases} \tag{8}$$

upstream: $$u_x = 0 \tag{9}$$

2.2 Numerical solution of the stress field

The boundary value problem was solved with the Finite Element package FEniCS (Alnæs et al., 2015) and stabilized with the Pressure Penalty method (Zhang et al., 2011). The numerical domain was divided into a regular triangular mesh with 100 vertical and 600 horizontal divisions.

Since the Stokes equation is linear in the stresses and the terminus boundary condition is linear in the ice thickness, the equations can be solved on a dimensionless domain and the stresses scaled to arbitrary ice thickness. Velocities do not scale linearly but can be obtained from the scaled stresses through the ice rheology equation. The water depth at the calving front was incorporated via the relative (dimensionless) water depth $w = D/H$.

In order to determine a suitable stress-criterion for cliff calving we consider a number of commonly used stresses which have a clear physical role (figure 2). [..[33]]Generally, stresses increase with ice thickness, while the presence of water at the glacier terminus decreases the stresses and stabilizes the calving front.

The deviatoric normal stress, S_{xx}, corresponds to an outwards force at the calving front which has two maxima, one at the waterline and one at the foot of the terminus. The deviatoric shear stress or Cauchy shear stress, ($S_{xz} = \sigma_{xz}$), translates to a bending moment which bends the top of the calving front forward and downward.

The different components of the deviatoric stress tensor are no invariants of the stress tensor, i.e. they depend on the coordinate system in which they are computed, and therefore they are not suitable as failure criteria. The largest principal stress,

$$\sigma_1 = \frac{\sigma_{xx} + \sigma_{zz}}{2} + \sqrt{\left(\frac{\sigma_{xx} - \sigma_{zz}}{2}\right)^2 + \sigma_{xz}^2}, \tag{10}$$

is calculated as the largest eigenvalue of the Cauchy stress tensor and corresponds to the largest normal stress in a given point. When σ_1 is positive, it is tensile and crevasses can form.

The maximum shear stress,

$$\tau_{max} = \sqrt{\left(\frac{\sigma_{xx} - \sigma_{zz}}{2}\right)^2 + \sigma_{xz}^2}, \tag{11}$$

[33]removed: In general, we find that

acts on a plane at an angle $45°$ to the plane where the largest principal stress acts. It has its maximum at the foot of the calving front. The maximum shear stress can be related to brittle compressive failure (Schulson, 2001) and is therefore of particular interest for cliff failure.

The von Mises stress [..[34]]is the second invariant J_2 of the deviatoric stress tensor,

$$\sigma_{Mises} = [..^{35}]\sqrt{\frac{3}{2}\left(\mathrm{S}_{xx}^2 + \mathrm{S}_{zz}^2 + 2\mathrm{S}_{xz}^2\right)}, \tag{12}$$

[..[36]]and is used as a measure of deviatoric strain energy. It can also be related to material failure (Ford and Alexander, 1963) and has been used as a calving criterion by Morlighem et al. (2016). [..[37]]Since $S_{xx} = -S_{zz}$ due to the incompressibility of ice, the von Mises stress and the maximum shear stress differ only by a factor: $\sigma_{Mises} = \sqrt{3}\tau_{max}$.

3 Cliff failure criterion

In a first step we select a failure criterion which then yields a failure region based on the computed stress fields. In a second step we decide on a time scale for the failure in order to derive a simple calving law.

3.1 Partial thickness failure through crevasses

Crevasses are a natural candidate for ice front failure. In the case of glaciers that are frozen to the ground, crevasses, generally, do not form from the base upward (Ma et al., 2017). Instead, surface crevasses can form in the upper part of the glacier down to the depth where the principal stress becomes compressive, i.e. attains negative values (Nye, 1957). The presence of water at the calving front reduces the stresses in the ice and decreases the depth to which surface crevasses can penetrate. Surface crevasses, generally, do not penetrate through the whole glacier thickness and so crevasses cannot be the sole cause for calving. We thus do not follow this path to determine a failure region.

Surface meltwater filling surface crevasses can increase their depth (hydrofracturing) (Weertman, 1973; Das et al., 2008; Pollard et al., 2015), but this is also not considered here. The presence of crevasses weakens the ice and is expected to enable failure even when the critical shear stress is not yet exceeded but also this is not further considered here. [..[38]]

3.2 Full thickness shear failure

[..[39]]

---

[34]removed: ,

[36]removed: is

[37]removed: Its distribution (not shown) is very similar to that of

[38]removed: Instead we consider the case of

[39]removed: The different components of the deviatoric stress tensor are no invariants of the stress tensor, i.e. they depend on the coordinate system in which they are computed, and therefore they are not suitable as failure criteria. The von-Mises stress is the second invariant J_2 of the deviatoric stress tensor and is frequently used as a failure criterion in material sciences (Ford and Alexander, 1963). However, it does not take into account whether deviatoric stresses are tensile or compressive or shear stresses and this is likely to be important for ice failure.

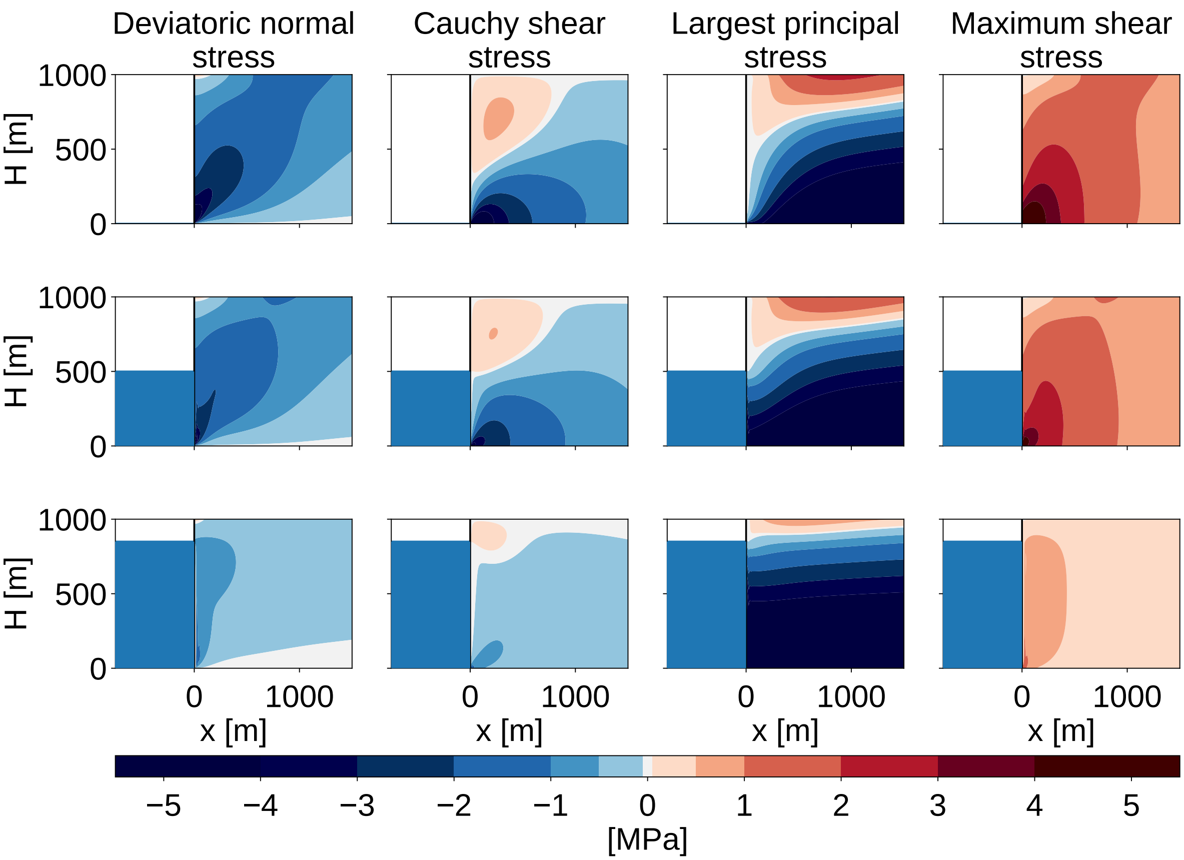

Figure 2. Stress configurations at the calving front for different relative water depths ($w = 0, 0.5, 0.85$) for a fixed ice thickness of 1000m. The first column shows the deviatoric normal stress in x-direction, S_{xx}, the second column shows the Cauchy shear stress, $\sigma_{xz} = S_{xz}$, the third column shows the largest principal stress, σ_i, and the last column shows the maximum shear stress, τ_{max}.

[..[40]]Instead, we assume shear faulting to be the dominant process in ice-cliff failure. We could use the von Mises stress as a failure criterion instead and reach qualitatively the same result, because they differ only by a factor of $\sqrt{3}$.

The failure region is defined as the region close to the calving front where the maximum shear stress exceeds a critical shear stress of $\tau_c = 1\,\mathrm{MPa}$ (Schulson et al., 1999; Schulson, 2001). While the specific value of the critical shear stress may be subject to [..[41]]uncertainties (values might be between $0.5\,\mathrm{MPa}$ and $5\,\mathrm{MPa}$), it is mainly a constant that will not alter the calving rate dependence on the freeboard and the water depth. The specific choice of the value is motivated by laboratory experiments and can only provide an order of magnitude of the calving rate. However, the uncertainty resulting from this choice is [..[42]]smaller than the uncertainty arising from the estimate of the failure time (see below).

[40]removed: Here

[41]removed: large uncertainties

[42]removed: probably not larger

3.3 Comparison to Coulomb failure

In general, brittle compressive failure happens through shear faulting (Schulson et al. (1999)) and can be described with the Coulomb law (Weiss and Schulson (2009)): the shear stress τ acting on the future fault plane is resisted by material cohesion S_0 and by friction $\mu\sigma$ with the friction coefficient μ and the normal stress across the failure plane σ. Failure happens, when:

$$\tau \geq S_0 + \mu\sigma \tag{13}$$

This expression depends on the direction of the fault plane. The failure condition can be expressed more generally in terms of the maximum shear stress τ_{max} and the isotropic pressure P as

$$\sqrt{\mu^2+1}\,\tau_{max} = \tau_0 + \mu P \tag{14}$$

where τ_0 is another measure of cohesive strength related to S_0 [..[43]](Weiss and Schulson (2009)).

Weiss and Schulson (2009) provide values of $\mu = 0.3 \ldots 0.8$ depending on the temperature of the ice. Since friction increases the strength of the ice, this could stabilize rather large ice cliffs. Bassis and Walker (2011) looked at upper bounds of glacier stability with a depth-averaged shear stress for different values of μ (0.65, 0.4, 0) and a cohesion of $\tau_0 = 1\,$MPa. With a large friction coefficient, ice cliffs would be stable for freeboards of up to $600\,$m (see fig. 3) Since this is not observed in nature, they concluded that the best model is the one without friction which only allows freeboards of up to $200\,$m. Thus with vanishing friction, the Coulomb failure criterion is equal to the maximum shear stress criterion used here.

4 Failure region

[..[46]]We define the failure region as the region close to the calving front where the maximum shear stress exceeds the critical shear stress τ_c anywhere in the ice column. The failure distance L is the maximum distance of the failure region to the front and was determined for a range of ice thicknesses H and relative water depths w by solving the 2D Stokes equation numerically and tracing the contour line where the maximum shear stress τ_{max} equals the critical shear stress τ_c (see figure 4).

For a given water depth, the [..[47]]failure distance L increases with the ice thickness H or the glacier freeboard $F = H - D$ (figure 5). For glacier freeboards smaller than approximately [..[48]]$100\,$m, the failure region vanishes: the critical shear stress is not exceeded anywhere in the ice and no shear failure takes place. This confirms results by Bassis and Walker (2011) which were derived analytically with some simplifications (see appendix A1 for more details). The relative water depths influences the slope of the freeboard - failure [..[49]]distance relation: for large relative water depths, the failure [..[50]]distance grows more quickly with increasing freeboard. This is because for a large relative water depth the overall ice thickness is much larger than for a similar freeboard with a smaller relative water depth and so the failure region is larger.

[43]removed: .
[46]removed: The maximum horizontal extend
[47]removed: extent of the failure region
[48]removed: 100m
[49]removed: region
[50]removed: region

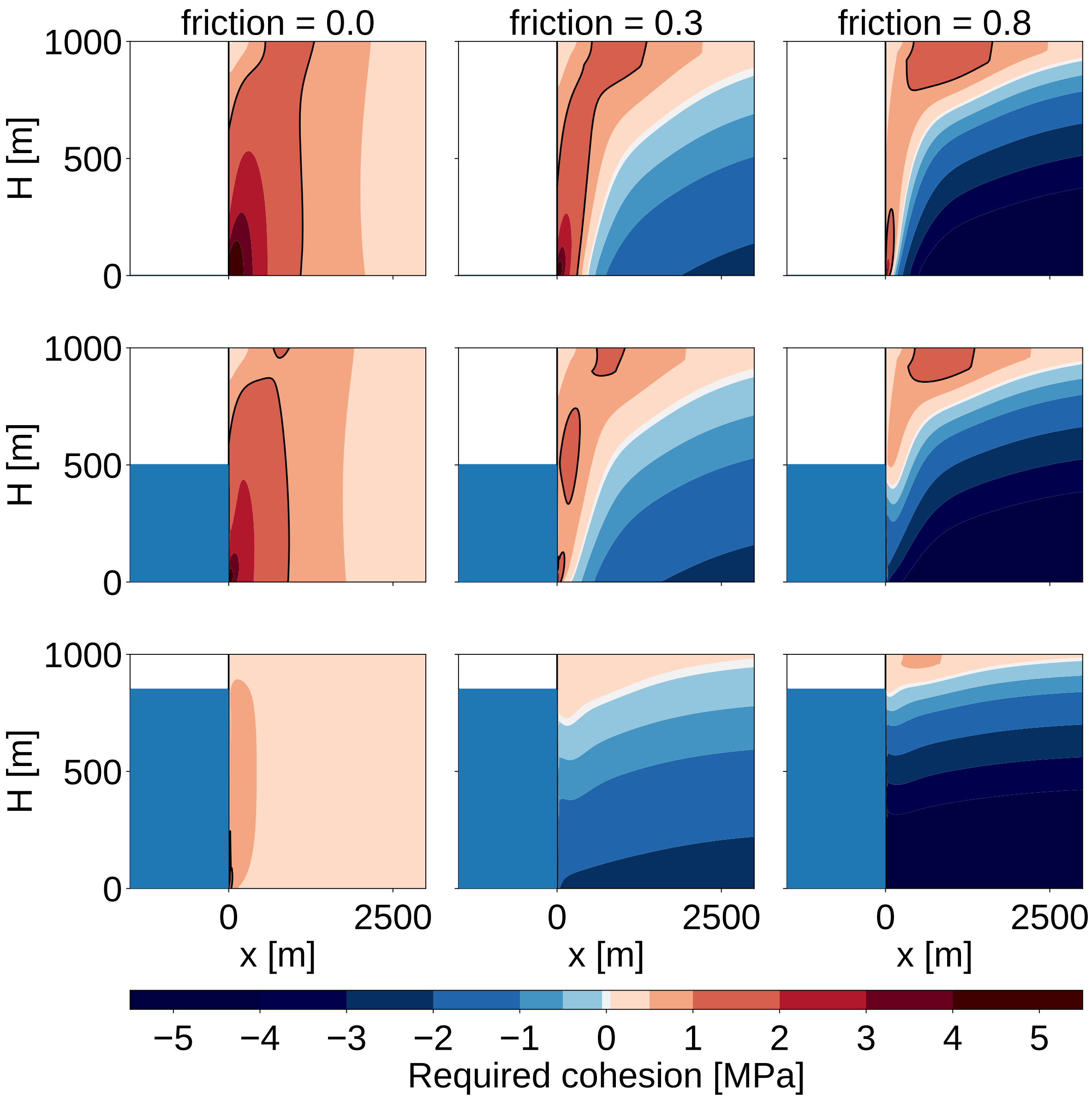

Figure 3. [..[44]]Assuming Coulomb failure, the required cohesion, $\tau_0 = \sqrt{\mu^2+1}\,\tau_{max} - \mu P$, is shown for different friction parameters ($\mu = 0, 0.3, 0.8$). The failure [..[45]]region for a maximum cohesion of $\tau_{max} = 1\,$Mpa is encased by the black line.

Above a critical freeboard of about $1000\,$m (see fig. 4 for $w = 0$ and $F = H$) the failure region encompasses the whole ice thickness. Below this critical value the failure region contains only the lower part of the ice thickness: but once the lower part

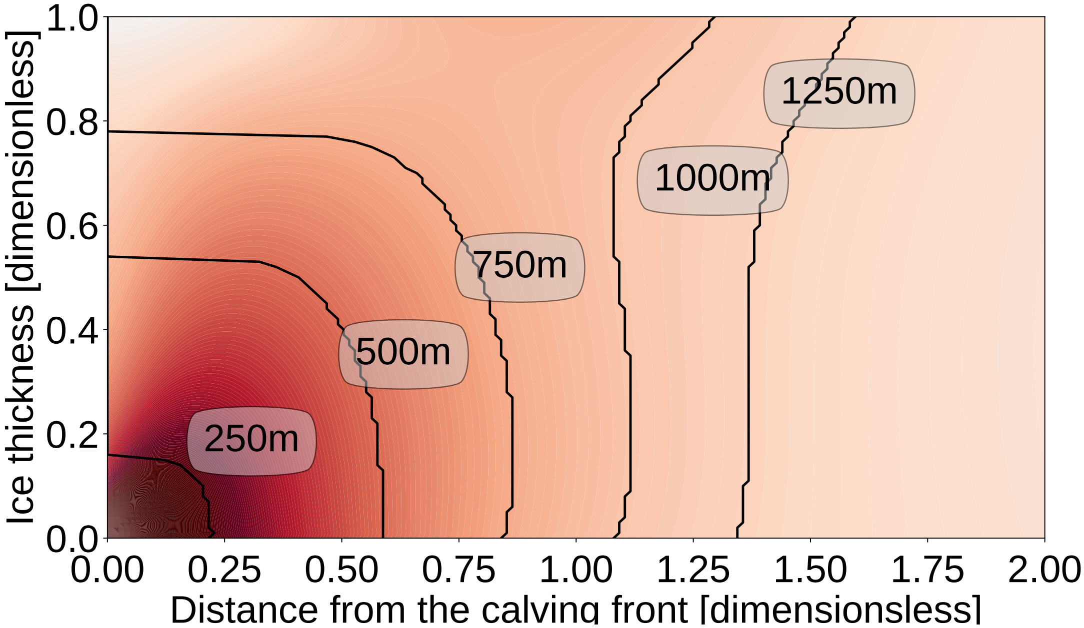

Figure 4. Outline of the failure region for different ice thicknesses on a dimensionless domain and without water stabilizing the front (ice thickness = glacier freeboard). The background color shows the maximum shear stress on a dimensionless scale with darker areas signifying larger stress. The failure region is defined as region close to the calving front where the maximum shear stress exceeds the critical shear stress τ_c anywhere in the ice column. The outline for $H = 1000\,\mathrm{m}$ is also shown in fig. 3 in the top-left panel.

of the ice column fails the upper part lacks support and fails as well. The [..[51]]freeboard - failure [..[52]]distance relation has a steeper slope for large freeboards when the whole ice thickness fails. This leads to a bend at the critical freeboard and hence the two parts require separate analytical fits. Here, we consider only values below the critical freeboard because that is the range of values most likely to occur in nature.

In figure 5 we provide an analytical fit with a power law function of the form

$$L = \left(\frac{F - F_c}{F_s}\right) [..^{53}]^{s}\,\mathrm{m} \tag{15}$$

$$F_s = \left(115 \cdot \left(w - [..^{54}]0.356\right)^4 + 21\right)\,\mathrm{m} \tag{16}$$

$$F_c = (75 - w \cdot 49)\,\mathrm{m} \tag{17}$$

$$s = 0.17 \cdot 9.1^{w} + 1.76 \tag{18}$$

[51] removed: freeobard

[52] removed: region

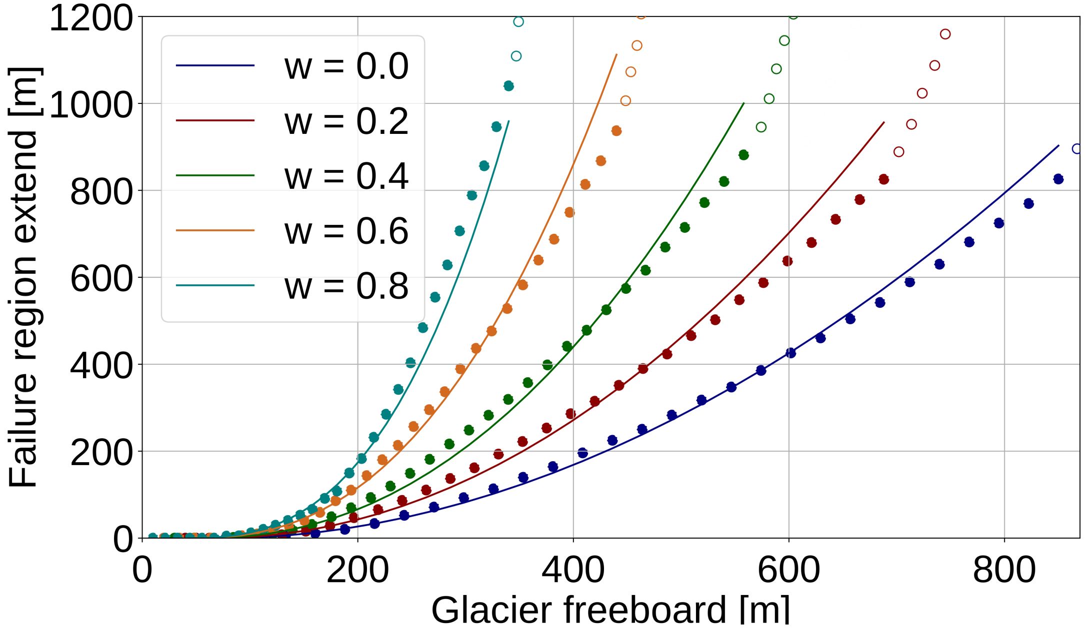

Figure 5. Size of shear failure region L as a function of glacier freeboard $F = H - D$ and relative water depth $w = D/H$[..[55]]. Numerical results are shown for smaller freeboards where the failure region does not encompass the whole ice thickness ([..[56]]filled dots) and for large freeboards, where the failure region contains the whole ice thickness (empty circles). A power law [..[57]]has been fitted to the numerical results for small freeboards (continuous line), which is given by eq. 15. The fit has been optimized for relative error in order to get the onset of cliff calving right.

with $w \equiv D/H < 0.9$ and $F \equiv H - D = H \cdot (1-w)$. At first L was fitted as a function of F for each value of w. Then the parameter functions F_s,F_c and s were fitted as functions of w.

Fig. 5 shows the numerical results and the fit. Note that the fit has been optimized for relative error so for large freeboards the fit is a little off but it was considered more important to fit the onset of cliff calving correctly.

5 Failure time

There is a theory for damage evolution in ice for tensile damage (Pralong et al., 2003), from which [..[58]]the time to failure [..[59]]is derived as (Mercenier et al., 2018):

$$T_f = \frac{(1-D_0)^{k+r+1} - (1-D_c)^{k+r+1}}{(k+r+1)B(\sigma_0 - \sigma_{th})^r} \tag{19}$$

[58] removed: a

[59] removed: can be derived

with the rate factor for damage evolution B, material constants r and k, initial damage D_0, critical damage D_c and stress threshold for damage creation σ_{th} and the working stress σ_0 which we assume to be the maximum shear stress τ_{max}. [..[60]]With these assumptions eq. 19 can be written as

$$\mathsf{T_f} = \cdot(\sigma_0 - \sigma_{\mathsf{th}})^{-\mathsf{r}}/\mathsf{B}^* \tag{20}$$

with $\sigma_{thr} = 0.17$MPa, [..[61]]$r = 0.43$ and $B^* = 65$Mpa^{-r}a^{-1}, as given in Mercenier et al. (2018). These parameters have been determined by calibrating a tensile failure calving model with data on calving rate, water depth and ice thickness for a variety of tidewater glaciers in the Arctic.

However, eq. 20 is valid only for damages created through tensile creep. The difference between tensile and compressive damage is that [..[62]]under tension a single crack grows [..[63]]in an unstable fashion to cause failure while in compression a large number of small crack grows [..[64]]in a stable fashion until their interaction causes failure (Ashby and Sammis, 1990).

There is plenty of literature about compressive creep and failure in rocks (Brantut et al., 2013). Fatigue failure happens when a material is loaded with stresses below the failure stress and fails with a time delay due to the development of micro cracks. There is an exponential law [..[65]]as well as a power law for the time to failure:

$$t_f = t_0 \exp\left(-b\frac{\sigma}{\sigma_0}\right) \tag{21}$$

$$t_f = t_0' \left(\frac{\sigma}{\sigma_0}\right) [..^{66}]^{-\mathsf{b}'} \tag{22}$$

The power law exponent is usually large, $b' \approx 20$, so the power law is very similar to the exponential law. [..[67]]Once the major stress σ exceeds the instantaneous strength σ_0, immediate failure is assumed ($t_f = 0$). Both time to failure relations fit the experimental data for rock well (Amitrano and Helmstetter, 2006). [..[68]]However, the constants depend on material properties [..[69]]and there are to our knowledge no studies for time dependence of compressive creep failure in ice. [..[70]]

This leaves us with a dilemma: There have been no studies that determined the material properties of ice under time-dependent brittle compressive failure. Also, we cannot determine those material properties ourselves by fitting the resulting calving law to observations, because so far cliff calving has not been observed as the major calving process in any glacier. That makes it impossible to estimate the time to failure [..[71]]

[..[72]]

---

[60] removed: However
[61] removed: this is strictly
[62] removed: in
[63] removed: unstably
[64] removed: stably
[65] removed: and
[67] removed: Both
[68] removed: The
[69] removed: . There are
[70] removed: Due to lack of data for time to failure in compressive failureof ice, we start with a
[71] removed: as given by eq. 19,

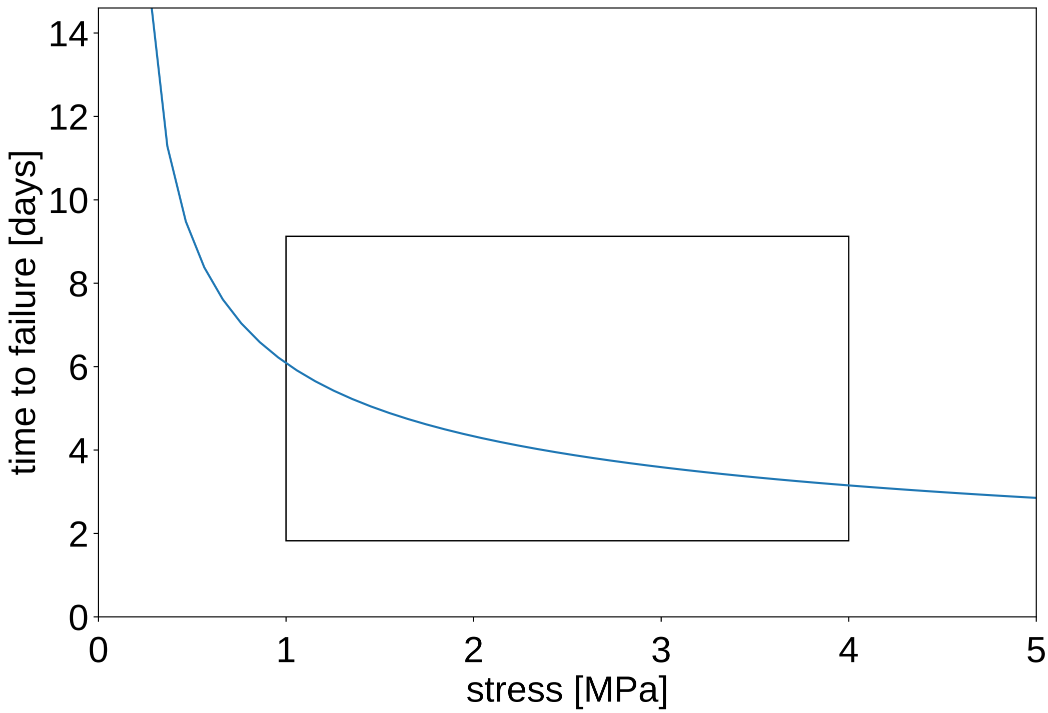

Figure 6. Time to failure given by eq. 20. For stresses above the shear failure threshold, $\sigma_0 > 1\,\mathrm{MPa}$, the time to failure changes only little (box).

[..[73]]using eq. 21 or 22. Eq. 20 and the value of its constants have been determined [..[74]]for tensile failure, which is microscopically very different from brittle compressive failure. So there is little reason to expect it to describe the timescale of shear failure well.

Nevertheless, we will use it as a starting point for our further analysis: For the stresses above the shear failure threshold, $\sigma_0 > 1\,\mathrm{MPa}$, the time to failure [..[75]]for tensile failure (given by eq. 20) changes by only a factor of 2 (see fig. 6). [..[76]]Hence, the calving relation can be further simplified by assuming [..[77]]that there is a characteristic time to failure, T_c, that is the same for all stresses and sizes of failure regions, $T_c \approx 4\,\mathrm{days}$. This characteristic time has been derived from parameters determined for tensile failure, so its application to shear failure comes with an uncertainty that is is difficult to quantify.

[73] removed: with $\sigma_{thr} = 0.17\,\mathrm{MPa}$, $r = 0.43$ and $B = 65\mathrm{Mpa}^{-r}\mathrm{a}^{-1}$, as given in Mercenier et al. (2018). These parameters

[74] removed: by calibrating a tensile failurecalving model with data on calving rate, water depth and ice thickness for a variety of tidewater glaciers in the Arctic.

[75] removed: given by this relation

[76] removed: The

[77] removed: ,

w	s	F_c	F_s
0	1.93	75	22.85
0.1	1.97	70.1	21.49
0.2	2.02	65.2	21.07
0.3	2.09	60.3	21.00
0.4	2.17	55.4	21.00
0.5	2.27	50.5	21.05
0.6	2.40	45.6	21.41
0.7	2.56	40.7	22.61
0.8	2.75	35.8	25.47
0.9	3.00	30.9	31.07

Table 1. Table of parameters in the cliff calving relation eq. 23, giving the exponent s, critical freeboard F_c and scaling factor F_s for a range of relative water depth values w.

6 Calving law

With a constant failure time, the calving rate is proportional to the size of the failure region

$$C = C_0 \cdot \left(\frac{F - F_c}{F_s}\right)^s \tag{23}$$

$$F_s = \left(115 \cdot \left(w - [..^{78}]0.356\right)^4 + 21\right)\,\mathrm{m} \tag{24}$$

$$F_c = (75 - w \cdot 49)\,\mathrm{m} \tag{25}$$

$$s = 0.17 \cdot 9.1^w + 1.76 \tag{26}$$

$$C_0 = \frac{1\,\mathrm{m}}{4\,\mathrm{days}} = 91.25\,\mathrm{ma}^{-1} \tag{27}$$

with $w \equiv D/H < 0.9$ and $F \equiv H - D = H \cdot (1 - w)$.

A dry cliff ($w = 0$) reaches calving rates of $C = 50$ km/a at an ice thickness of $F = H \approx 800$ m, while an ice cliff that is close to floatation ($w = 0.8$) reaches the same calving rate at a freeboard of $F \approx 300$ m, which corresponds to an ice thickness of $H \approx 1500$ m (see fig. 7).

How do cliff calving rates given by eq. 23 compare to currently observed calving rates? A glacier enters the cliff calving regime, when its freeboard is larger than the critical freeboard F_c and the cliff calving rate given by eq. 23 becomes nonzero. Obviously, glaciers calve through tensile failure before and after they reach the cliff calving regime, so we expect the overall calving rate to be larger than the cliff calving rate, especially for glaciers that just entered the cliff calving regime and are heavily crevassed.

Jakobshavn glacier in Greenland is one of the few glacier that are currently in a cliff calving mode. Jakobshavn glacier terminates in water with a depth of 800 m (Morlighem et al., 2014) and has a glacier freeboard of 100 m (Xie et al., 2018). Therefore it can be considered to be at the beginning of the cliff calving regime. Since the terminus is also heavily

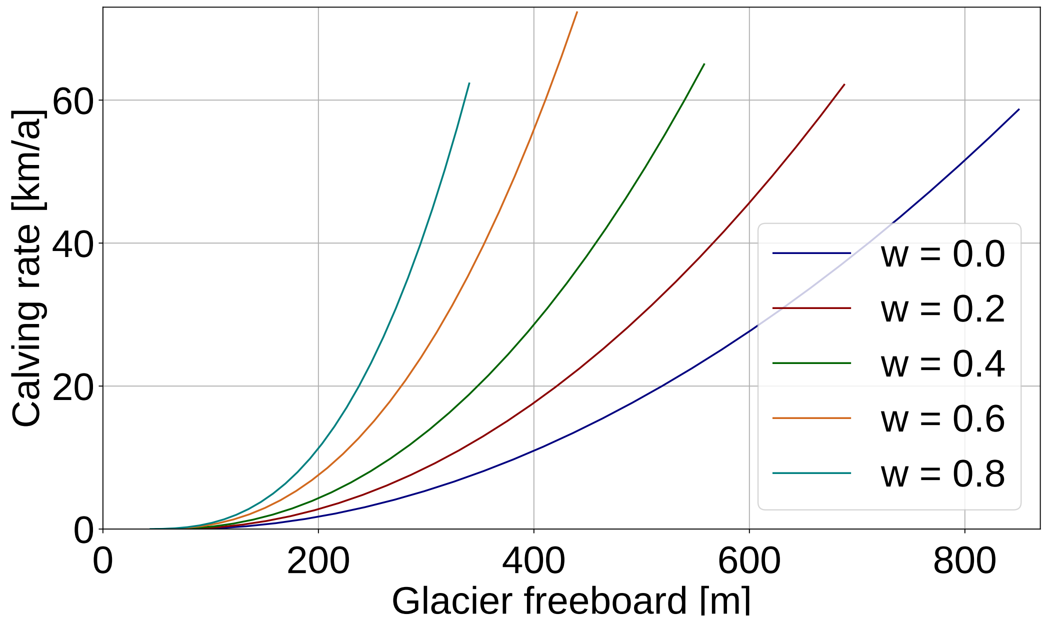

Figure 7. Cliff calving rates C as a function of glacier freeboard $F = H - D$ and relative water depth $w = D/H$ as given by eq. 23.

crevassed, we expect tensile calving to be the main contribution to the overall calving rate. Hence, this example can only give an upper bound on the possible cliff calving rate.

It is difficult to [..[79]]determine calving rates directly. The ice flow velocity [..[80]]to the front of Jakobshavn is up to $12\,\mathrm{kma}^{-1}$ (Morlighem et al., 2014). The grounding line of Jakobshaven glacier retreats and advances seasonally about $6\,\mathrm{km}$ per year, but the maximum grounding line position has not changed much between 2012 and 2015 (Xie et al., 2018). [..[81]]Assuming a fixed grounding line, the calving rate would equal the flow velocity. Hence the averaged yearly calving rate is approximately $12\,\mathrm{kma}^{-1}$. [..[82]]

Inserting values of glacier freeboard and water depth given above into eq. 23 gives a cliff calving rate of $C = 750\,\mathrm{ma}^{-1}$, which is well below the overall calving rate. [..[83]]

[79] removed: determine calving rates directly, but if the grounding line were fixed, the calving rate would be equal to the

[80] removed: which

[81] removed: So

[82] removed: Jakobshavn glacier terminates in water with a depth of $800\,\mathrm{m}$ (Morlighem et al., 2014) and has a glacier freeboard of $100\,\mathrm{m}$ (Xie et al., 2018). That brings Jakobshavn glacier in the cliff calving regime. Inserting these values

[83] removed: Jakoshavn glacier is heavily crevassed so other calving mechanism are likely to play a role and the cliff calving rate is only a part of the whole calving rate.

6.1 [..[84]]

7 Discussion and Conclusion

We solved the 2D Stokes equation numerically for a flat glacier frozen to its bed in a [..[85]]flow-line model and investigated the stresses at the calving front.

Four simplifications were made:

1. The model was solved in one horizontal direction, neglecting lateral shear effects. Without lateral shear effects, the result is [..[86]]independent of the topography of individual glaciers.
2. We assumed a basal boundary condition corresponding to a glacier frozen to its bed. Sliding was not considered.
3. The main failure mechanism was assumed to be shear faulting[..[87]]. We assumed brittle compressive failure according to the Coulomb law [..[88]]without friction stabilizing the ice cliff. Friction would allow glaciers with larger freeboards than observed to be stable.
4. A constant time to failure has been assumed.

Under these assumptions, crevasses cannot penetrate the whole glacier depth and shear failure was chosen as the main failure mechanism. The region where shear stresses exceed a critical shear stress of 1 MPa is called the failure region. The extend of this failure region, the failure distance, was determined for a range of glacier freeboards and relative water depths. [..[89]]For freeboards small enough for the failure region [..[90]]not to encompass the whole ice thickness, an analytical fit was made. Assuming a constant time to failure, a cliff calving rate was derived. Resulting cliff calving rates seem large compared to currently observed calving rates[..[91]]. Comparison with Jakobshavn glacier in Greenland [..[92]]shows that the cliff calving rate is smaller than the overall calving rate, [..[93]]hence we conclude that eq. 23 probably does not overestimate cliff calving rates.

7.1 Idealized setup vs. realistic conditions

The cliff calving rate was derived using an idealized setup, given by the first two of the four assumptions described above. Realistic glaciers that might experience cliff calving sit in valleys where they experience lateral drag and may be sliding. The calving front may have a slope rather than a vertical cliff and there might be an undercut caused by frontal melt.

[84] removed: Discussion and Conclusion
[85] removed: flowline
[86] removed: indepenent
[87] removed: without friction compared
[88] removed: , where friction which ice cliffs
[89] removed: Where
[90] removed: does not
[91] removed: , but comparison
[92] removed: , where cliff calving contributes to
[93] removed: shows that it can be realistic. However, cliff calving rates increase quickly with increasing glacier freeboard and glaciers in a true

7.1.1 Sliding glaciers

First consider sliding with a constant velocity v (i.e. vanishing strain rate) for which the upstream boundary condition is an influx with velocity v, so $u = v$. The basal boundary conditions become $u = v$, $w = 0$. Solving the Stokes' equations with these boundary conditions numerically with FeniCS gives the exact same stress fields as in the frozen case and the velocity field is simply shifted by the sliding velocity v. This is not surprising: A simple Galilean transformation takes this sliding glacier back to the frozen glacier previously considered without changing any of the physics.

In general, sliding velocities increase towards the glacier terminus. The steepest possible velocity gradient can be obtained with a free-slip basal boundary condition: we assume no influx at the upstream boundary, $u = 0$, and at the bed we assume free slip in the horizontal direction, which only leaves a boundary condition for the vertical velocity, $w = 0$. The basal velocity is zero at the upstream boundary and takes its maximum at the calving front. Due to this velocity gradient, the maximum shear stress is large throughout the whole numerical domain (see fig. 8). For increasing ice thickness it becomes difficult to define a meaningful failure region, because the critical shear stress is exceeded in the whole numerical domain - one must assume that the whole numerical domain will fail. Thus, in the case of a sliding glacier, the failure region is larger than in the case of a glacier frozen to its bed. Hence, the derived cliff calving rate can serve as a lower bound for this kind of calving fronts.

To summarize: The derived cliff calving law is valid for glaciers that are frozen to the bed or sliding with a constant velocity and vanishing strain rate. It serves as a lower bound on the calving rate for glaciers in which velocities increase towards the calving front.

7.1.2 Lateral drag

In order to investigate how lateral drag influences cliff calving, we will assume ice flow in a channel with a flow-line in the x-direction. Ice is assumed to flow only in the x-direction with a flow maximum in the middle of the channel. Since deviatoric stresses are connected to the strain rate, $\tau_{ij} = B\dot{\epsilon}_e\dot{\epsilon}_{ij}$, and the strain rate is given by the velocity gradients, $\dot{\epsilon}_{ij} = \frac{1}{2}\left(\partial_i u_j + \partial_i u_j\right)$, we get an additional deviatoric shear stress in the x-y-plane, τ_{xy}. The other stress components in y vanish, $\tau_{yz} = \tau_{yy} = 0$, because the respective velocity gradients vanish. The Cauchy stress tensor becomes

$$\sigma = \begin{pmatrix} P + \tau_{xx} & \tau_{xy} & \tau_{xz} \\ \tau_{xy} & P & 0 \\ \tau_{xz} & 0 & P - \tau_{xx} \end{pmatrix} \tag{28}$$

The principal stresses σ_i are defined as eigenvalues of σ, and the maximum shear stress τ_{max} as the the difference between the maximum and minimum principal stress. In 3D, there is no simple analytical formula for the eigenvalues of a matrix and therefore it is not feasible to get an analytical estimate on whether the introduction of non-zero τ_{xy} makes τ_{max} smaller or larger.

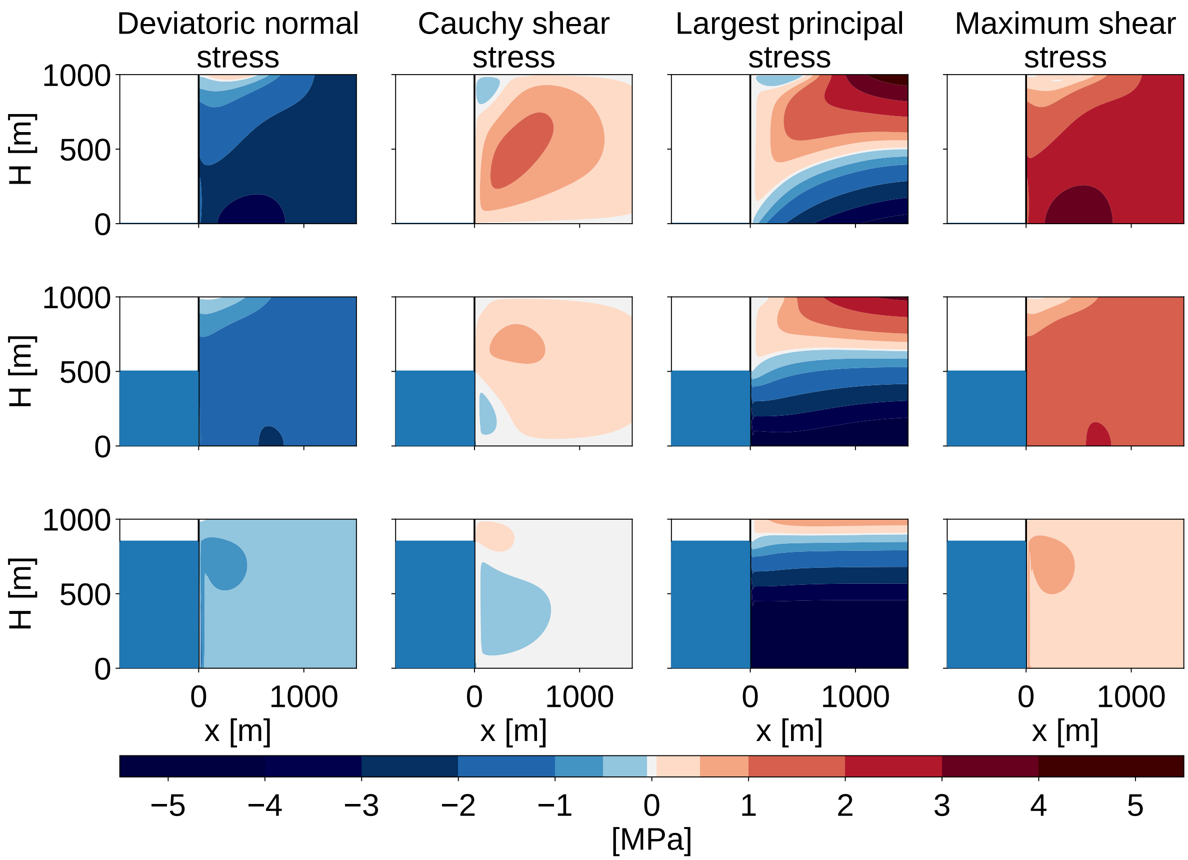

Figure 8. Stress configurations at the calving front for different relative water depths ($w = 0, 0.5, 0.85$) for a fixed ice thickness of 1000m with a free-slip basal boundary condition instead of the no-slip boundary condition used in the previous analysis (compare fig. 2). The first column shows the deviatoric normal stress in x-direction, S_{xx}, the second column shows the Cauchy shear stress, $\sigma_{xz} = S_{xz}$, the third column shows the largest principal stress, σ_i, and the last column shows the maximum shear stress, τ_{max}. In contrast with the no-slip case, there is no definite failure region as the maximum shear stress is large throughout the whole numerical domain.

Assuming $P(x,z)$, $\tau_{xx}(x,z)$ and $\tau_{xz}(x,z)$ as given by the FeniCS simulation with a constant $\tau_{xy} = 1$ MPa, we calculate the principal stresses and the maximum shear stress numerically. This shows that τ_{max} increases with increasing absolute value of τ_{xy} (see fig. 9).

Hence, lateral shear increases the maximum shear, therefore increasing the size of the failure region and the cliff calving rate. The derived cliff calving rate can serve as a lower bound if lateral drag is present.

7.1.3 Calving front slope

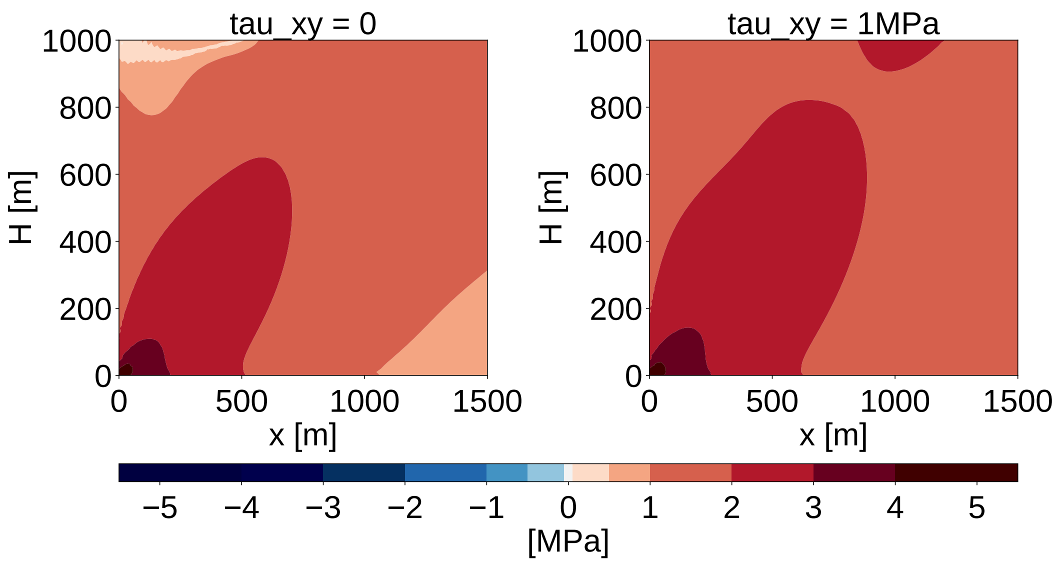

Figure 9. Maximum shear stress τ_{max} in the vicinity of the calving front in the case without lateral drag (left) and with a constant lateral drag of $\tau_{xy} = 1$ MPa (right).

Other studies have shown that a calving front with a slope has significantly reduced stresses compared to a calving front with a vertical cliff (Benn et al., 2017; Mercenier et al., 2018). It is clear that a calving front slope would also reduce the cliff calving rate.

We have not analyzed this effect here, because once cliff calving has been initiated, the full thickness calving probably prevents calving front slopes from forming. We aim to find a parametrization that can be implemented in ice sheet models capable of simulating the Antarctic ice sheet. These simulations are done on resolutions of several kilometers and cannot resolve calving front slopes on length scales of several tens or hundreds of meters.

7.1.4 Melt-undercut

Undercut from melt would increase the stresses near the calving front (Benn et al., 2017) and hence increase the calving rate.

7.2 Uncertainties

Cliff calving is still a rather hypothetical process with a very limited scope of observations. Since there are currently no glaciers that are clearly in a cliff calving regime[..[94]], the calving rate cannot be fitted to observed calving rates. There is uncertainty in the maximum shear stress used to determine the failure distance as well as the time to failure.

[94]removed: can retreat much faster than has been observed so far.

Laboratory studies give a range of values between 0.5 MPa and 5 MPa (Schulson et al., 1999; Schulson, 2001). A much larger uncertainty arises from the time to failure. There are studies that give time to failure relations and parameters for brittle compressive of rocks, but none for ice. Time to failure of ice has only been studied for tensile failure. We use the time to failure relation used by Mercenier et al. (2018) as a first guess. Applying this time to failure for tensile failure to a process of shear failure is very uncertain. We guess that the time to failure could be up to an order of magnitude smaller or larger.

The scaling parameter C_0 in eq. 23 should therefore be considered a free parameter. In any implementation of this cliff calving relation, a range of values for C_0 should be tested for plausibility.

7.3 Comparison with other calving parametrisations

7.3.1 Other cliff calving approaches

Bassis and Walker (2011) derived a stability limit for ice cliffs considering shear and tensile failure (their assumptions are analyzed further in the appendix). According to eq. 23, cliff calving starts when the freeboard is above $F \approx 75$ m, this is close to the stability limit of $F \approx 100$ m given by Bassis and Walker (2011).

Pollard et al. (2015) and DeConto and Pollard (2016) implemented cliff calving in their ice sheet model by assuming a cliff calving rate that is zero until the freeboard has reached ≈ 100 m, increases linearly up to 3 km/a for a freeboard of about 2000 m and stays constant after that. The calving relation is modified by factors representing back stress and additional wet-crevasse deepening. Edwards et al. (2019) did an ensemble study with a range of values for the maximum cliff calving rate from 0 km/a (no cliff calving) up to 5 km/a. If a scaling constant of $C_0 = 10$ m/a is used, cliff calving rates given by eq. 23 have an equal range of magnitude, but increase with a power-law dependence rather than linearly and have no upper bound.

Bassis et al. (2017) implemented cliff calving by requiring that ice cliffs cannot exceed the stability limit. This becomes a condition for the speed of grounding line retreat and advance. Eq. 23 is easier to implement in ice sheet models, because it can be implemented just like other calving parametrizations and does not need to be rewritten as a condition for the grounding line.

7.3.2 Other stress-based calving laws

Mercenier et al. (2018) derived a cliff calving law for tidewater glaciers below the stability limit by solving the stresses in the vicinity of the front and assuming tensile failure through the formation of a large crevasse. In contrast, we assume shear failure (also called brittle compressive failure). The calving rate given by Mercenier et al. (2018) increases approximately linearly with the freeboard and has no lower bound, while the calving rate given by eq. 23 grows with a power $s(w) > 1$ for freeboards larger than the critical freeboard $F_c(w)$ (see fig. 10). Hence, we expect tensile failure to dominate for small freeboards and shear failure to dominate for large freeboards.

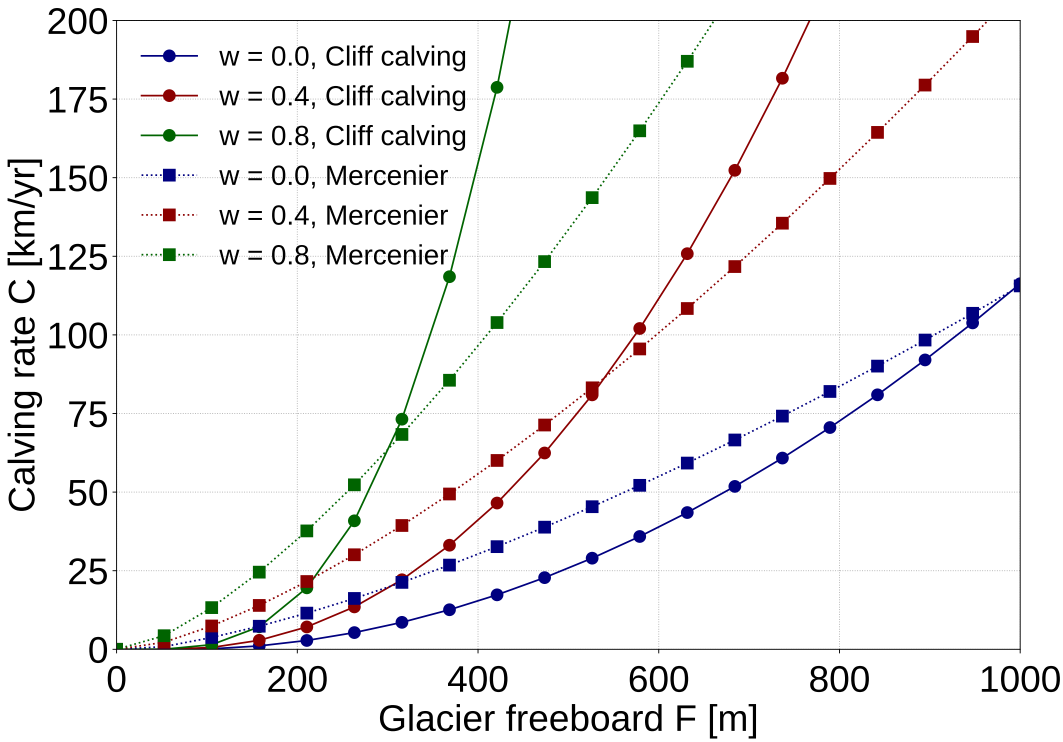

Figure 10. Comparison of the cliff calving law given by eq. 23 (continuous line) with the calving law for tidewater glaciers given by Mercenier et al. (2018), eq. 22 (dotted line). Note that the cliff calving rate could be scaled differently due to the uncertainty in C_0

.

It is difficult to say at which glacier freeboard the tensile failure regime ends and the shear failure regime begins, not only due to uncertainty in the scaling parameter C_0. In practice, both failure modes will interact, with tensile stress damaging the ice through few large crevasses originating from the surface of the ice and shear stress damaging the ice through a large number of small crevasses in the lower part of the cliff. This likely interaction of failure modes cannot be analyzed by assuming ice to be a continuous medium (like the approach used here and by Mercenier et al. (2018)), but should be done with damage theory or a discrete element approach.

7.4 Conclusion

The calving law proposed here was derived under a number of constraining assumptions. First it was assumed that friction plays no role in shear failure. Secondly it was assumed that once the critical shear stress is exceeded, ice fails after a constant time to failure. An improved cliff calving model might include friction and allow a stress-dependent time to failure.

If the Coulomb law with a friction component is used, the immediate failure region is smaller than in the no-friction case. Time to failure relations for compressive failure as given by 21 and 22 are valid for stresses below the critical shear stress.

Failure is assumed to be instantaneous as soon as the critical shear stress is reached. Regions where the stress is below the failure stress would be assigned a stress-dependent failure time leading to a spatially distributed time to failure. Since friction is smaller at the top of the ice cliff, the top would fail earlier than the base, leaving a foot that would subsequently fail due to buoyant forces. There is no simple way to find a parametrization of the cliff calving rate for these processes.

Another problem is that there are no laboratory studies on the [..[95]]parameters in the time to failure relations for ice. It is also not possible to calibrate the calving relation using observed calving rates, because there are no glaciers currently available where cliff calving is the primary failure mechanism. Paleorecords might provide some means to calibrate cliff-calving rates as attempted in Pollard et al. (2015) and DeConto and Pollard (2016).

Paleorecords might not be constraining enough to provide a useful limit for the Antarctic sea level contribution of the next 85 years. But even if it is difficult to constrain the rate of cliff-calving there are important qualitative consequences of a monotonously increasing cliff-calving dependence on ice thickness. The most important is the potential of a self-amplifying ice loss mechanism which is not constraint by the reduction in calving but must be constraint by other processes. Without some kind of cliff-calving mechanism it is likely that ice sheet models are lacking an important ice loss mechanism.

Code availability. FeniCS can be downloaded from the project website https://fenicsproject.org/download/. The script used for the FeniCS simulation in this paper is available on request from the authors.

Appendix A: Simplified stress balance

It is possible to solve the stress balance at the calving front analytically in a depth-averaged model with a simplifying assumption for the isotropic pressure. This has been used by (Bassis and Walker, 2011) and (Pollard et al., 2015). It is interesting to compare this with the numerical stress field solution obtained above.

(Bassis and Walker, 2011) and (Pollard et al., 2015) assumed the isotropic pressure is given by the gravitational pressure

$$P(x,z) = \rho_i g(H - z) \tag{A1}$$

where ρ_i is the density of ice. This assumption is actually only true over length scales that are large compared with the ice thickness and far from the ice margins (MacAyeal, 1989), which is not the case when stresses close to the calving front are [..[96]]analyzed. But making this assumption allows for an analytical solution of the depth-averaged stresses and does not require any ice rheology. [..[97]]

[95] removed: paramaters

[96] removed: analysed

[97] removed: Together with incrompessibilty

Together with incompressibility, which means that the trace of the strain rate disappears ($\dot{\epsilon}_{kk} = 0$) and implies $S_{xx} + S_{zz} = 0$, the 2D Stokes equations become:

$$0 = \frac{\partial S_{xx}}{\partial x} + \frac{\partial S_{xz}}{\partial z}\,, \tag{A2}$$

$$0 = \frac{\partial S_{xz}}{\partial x} - \frac{\partial S_{xx}}{\partial z}\,. \tag{A3}$$

Assuming a [..[98]]traction-free surface boundary, traction-continuity at the terminus boundary and vanishing deviatoric stresses at the upstream boundary as well as the bed boundary, a boundary value problem arises that can be solved numerically.

The resulting stresses are smaller than the stresses obtained in the section 2 for the 2D Stokes equation with nonlinear ice rheology (figure A1). A failure region can be defined as in section 3 and its size shows a very similar dependence on glacier freeboard and water depth, though it is smaller by about a factor of three.

The biggest difference between the two approaches lies in the largest principal stress: In this simplified problem, the largest principal stress is negative in the whole ice volume; there is no region of tensile stresses, so no crevasses form. This is due to the assumption that the isotropic pressure is equal to the gravitational pressure, which is not actually the case in the vicinity of the glacier terminus.

Competing interests. The authors declare no competing interests.

Acknowledgements. TS was funded by the Heinrich Böll Foundation. TS would like to thank Yue Ma and Christian Helanow for their valuable help with FeniCS.

[98] removed: tractionfree

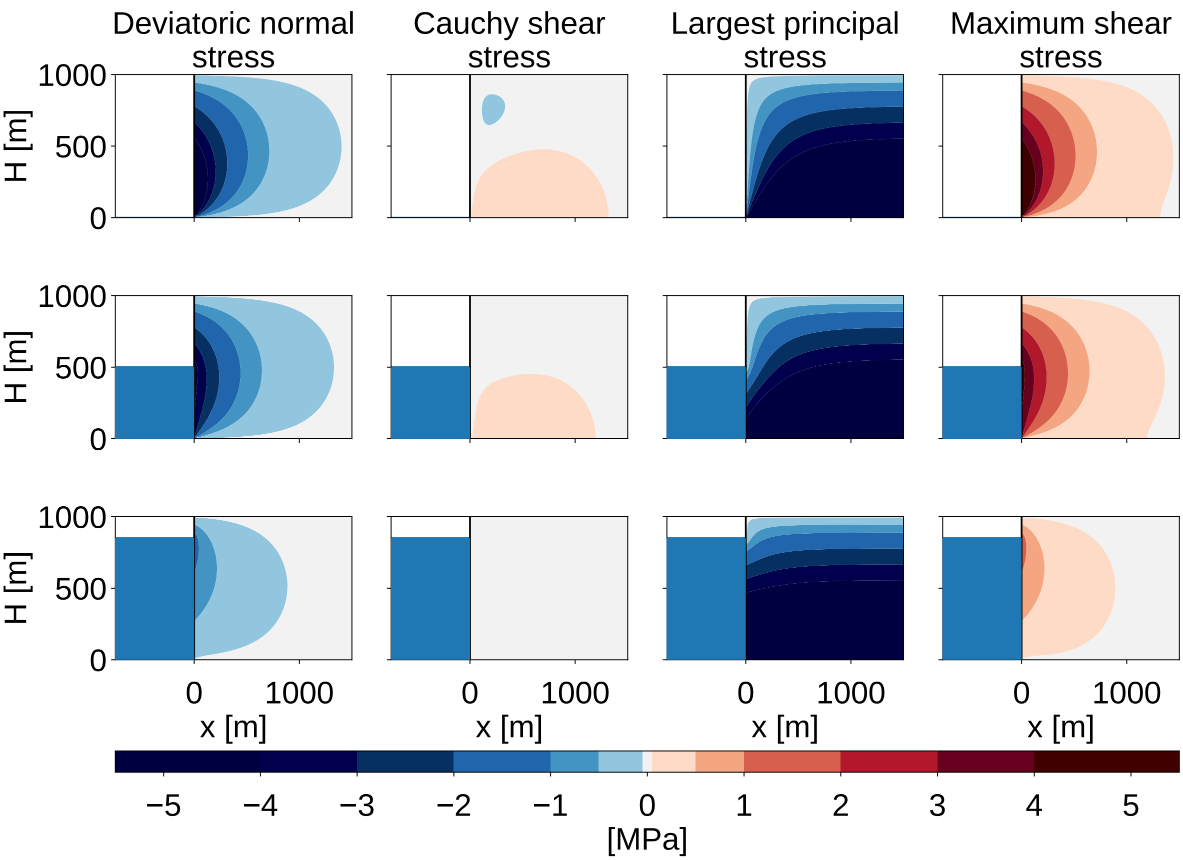

Figure A1. Stress configurations at the calving front for different relative water depths ($w = 0, 0.5, 0.85$) for a fixed ice thickness of 1000m. The first row shows the deviatoric normal stress in x-direction, S_{xx}, the second row shows the Cauchy shear stress, $\sigma_{xz} = S_{xz}$, the third row shows the largest principal stress, σ_i, and the last row shows the maximum shear stress, τ_{max}.

References

Alnæs, M. S., Blechta, J., Hake, J., Johansson, A., Kehlet, B., Logg, A., Richardson, C., Ring, J., Rognes, M. E., and Wells, G. N.: The FEniCS Project Version 1.5, Archive of Numerical Software, 3, https://doi.org/10.11588/ans.2015.100.20553, 2015.

Amitrano, D. and Helmstetter, A.: Brittle creep, damage, and time to failure in rocks, Journal of Geophysical Research: Solid Earth, 111, https://doi.org/10.1029/2005JB004252, https://agupubs.onlinelibrary.wiley.com/doi/abs/10.1029/2005JB004252, 2006.

Ashby, M. F. and Sammis, C. G.: The damage mechanics of brittle solids in compression, pure and applied geophysics, 133, 489–521, https://doi.org/10.1007/BF00878002, https://doi.org/10.1007/BF00878002, 1990.

Bassis, J. N. and Walker, C. C.: Upper and lower limits on the stability of calving glaciers from the yield strength envelope of ice, Proceedings of the Royal Society of London A: Mathematical, Physical and Engineering Sciences, https://doi.org/10.1098/rspa.2011.0422, http://rspa.royalsocietypublishing.org/content/early/2011/11/17/rspa.2011.0422, 2011.

Bassis, J. N., Petersen, S. V., and Mac Cathles, L.: Heinrich events triggered by ocean forcing and modulated by isostatic adjustment, Nature, 542, 332, https://doi.org/10.1038/nature21069, 2017.

Benn, D., Astrom, J., Zwinger, T., Todd, J., Nick, F., Cook, S., Hulton, N., and Luckmann, A.: Melt-under-cutting and buoyancy-driven calving from tidewater glaciers: new insights from discrete element and continuum model simulations, Journal of Glaciology, 63, 691–702, https://doi.org/10.1017/jog.2017.41, 2017.

Benn, D. I., Warren, C. R., and Mottram, R. H.: Calving processes and the dynamics of calving glaciers, Earth-Science Reviews, 82, 143–179, https://doi.org/10.1016/j.earscirev.2007.02.002, http://www.sciencedirect.com/science/article/pii/S0012825207000396, 2007.

Brantut, N., Heap, M., Meredith, P., and Baud, P.: Time-dependent cracking and brittle creep in crustal rocks: A review, Journal of Structural Geology, 52, 17 – 43, https://doi.org/https://doi.org/10.1016/j.jsg.2013.03.007, http://www.sciencedirect.com/science/article/pii/S0191814113000473, 2013.

Church, J. A., Clark, P. U., Cazenave, A., Gregory, J. M., Jevrejeva, S., Levermann, A., Merrifield, M. A., Milne, G. A., Nerem, R. S., Nunn, P. D., Payne, A. J., Pfeffer, W. T., Stammer, D., and Unnikrishnan, A. S.: Sea-Level Rise by 2100, Science, 342, 1445–1445, https://doi.org/10.1126/science.342.6165.1445-a, http://science.sciencemag.org/content/342/6165/1445.1, 2013.

Das, S. B., Joughin, I., Behn, M. D., Howat, I. M., King, M. A., Lizarralde, D., and Bhatia, M. P.: Fracture Propagation to the Base of the Greenland Ice Sheet During Supraglacial Lake Drainage, Science, 320, 778–781, https://doi.org/10.1126/science.1153360, http://science.sciencemag.org/content/320/5877/778, 2008.

DeConto, R. M. and Pollard, D.: Contribution of Antarctica to past and future sea-level rise, Nature, 531, 591–597, https://doi.org/http://dx.doi.org/10.1038/nature17145 10.1038/nature17145, http://www.nature.com/nature/journal/v531/n7596/abs/nature17145.html#supplementary-information, 2016.

Depoorter, M. A., Bamber, J. L., Griggs, J. A., Lenaerts, J. T. M., Ligtenberg, S. R. M., van den Broeke, M. R., and Moholdt, G.: Calving fluxes and basal melt rates of Antarctic ice shelves, Nature, 502, 89, http://dx.doi.org/10.1038/nature12567, 2013.

Edwards, T. L., Brandon, M. A., Durand, G., Edwards, N. R., Golledge, N. R., Holden, P. B., Nias, I. J., Payne, A. J., Ritz, C., and Wernecke, A.: Revisiting Antarctic ice loss due to marine ice-cliff instability, Nature, 566, 58–64, https://doi.org/10.1038/s41586-019-0901-4, 2019.

Enderlin, E. M., Howat, I. M., Jeong, S., Noh, M.-J., Angelen, J. H., and Broeke, M. R.: An improved mass budget for the Greenland ice sheet, Geophysical Research Letters, 41, 866–872, https://doi.org/10.1002/2013GL059010, https://agupubs.onlinelibrary.wiley.com/doi/abs/10.1002/2013GL059010, 2014.

Ford, H. and Alexander, J. M.: Advanced mechanics of materials, 1963.

Jiménez, S. and Duddu, R.: On the evaluation of the stress intensity factor in calving models using linear elastic fracture mechanics, Journal of Glaciology, 64, 759–770, https://doi.org/10.1017/jog.2018.64, 2018.

Joughin, I. and MacAyeal, D. R.: Calving of large tabular icebergs from ice shelf rift systems, Geophysical Research Letters, 32, n/a–n/a, https://doi.org/10.1029/2004GL020978, http://dx.doi.org/10.1029/2004GL020978, l02501, 2005.

Kopp, R. E., DeConto, R. M., Bader, D. A., Hay, C. C., Horton, R. M., Kulp, S., Oppenheimer, M., Pollard, D., and Strauss, B. H.: Evolving Understanding of Antarctic Ice-Sheet Physics and Ambiguity in Probabilistic Sea-Level Projections, Earth's Future, 5, 1217–1233, https://doi.org/10.1002/2017EF000663, https://agupubs.onlinelibrary.wiley.com/doi/abs/10.1002/2017EF000663, 2017.

Krug, J., Weiss, J., Gagliardini, O., and Durand, G.: Combining damage and fracture mechanics to model calving, The Cryosphere, 8, 2101–2117, 2014.

Lazzara, M. A., Jezek, K. C., Scambos, T. A., MacAyeal, D. R., and van der Veen, C. J.: On the recent calving of icebergs from the Ross Ice Shelf, Polar Geography, 23, 201–212, https://doi.org/10.1080/10889379909377676, http://dx.doi.org/10.1080/10889379909377676, 1999.

Levermann, A., Winkelmann, R., Nowicki, S., Fastook, J. L., Frieler, K., Greve, R., Hellmer, H. H., Martin, M. A., Meinshausen, M., Mengel, M., Payne, A. J., Pollard, D., Sato, T., Timmermann, R., Wang, W. L., and Bindschadler, R. A.: Projecting Antarctic ice discharge using response functions from SeaRISE ice-sheet models, Earth System Dynamics, 5, 271–293, https://doi.org/10.5194/esd-5-271-2014, https://www.earth-syst-dynam.net/5/271/2014/, 2014.

Ma, Y., Tripathy, C. S., and Bassis, J. N.: Bounds on the calving cliff height of marine terminating glaciers, Geophysical Research Letters, 44, 1369–1375, https://doi.org/10.1002/2016GL071560, http://dx.doi.org/10.1002/2016GL071560, 2016GL071560, 2017.

MacAyeal, D. R.: Large-scale ice flow over a viscous basal sediment: Theory and application to ice stream B, Antarctica, Journal of Geophysical Research: Solid Earth, 94, 4071–4087, https://doi.org/10.1029/JB094iB04p04071, http://dx.doi.org/10.1029/JB094iB04p04071, 1989.

Meier, M. F. and Post, A.: Fast tidewater glaciers, Journal of Geophysical Research: Solid Earth, 92, 9051–9058, https://doi.org/10.1029/JB092iB09p09051, http://dx.doi.org/10.1029/JB092iB09p09051, 1987.

Mengel, M., Feldmann, J., and Levermann, A.: Linear sea-level response to abrupt ocean warming of major West Antarctic ice basin, Nature Climate Change, 6, 71, http://dx.doi.org/10.1038/nclimate2808, 2016.

Mercenier, R., Lüthi, M. P., and Vieli, A.: Calving relation for tidewater glaciers based on detailed stress field analysis, The Cryosphere, 12, 721–739, https://doi.org/10.5194/tc-12-721-2018, https://www.the-cryosphere.net/12/721/2018/, 2018.

Morlighem, M., Rignot, E., Mouginot, J., Seroussi, H., and Larour, E.: Deeply incised submarine glacial valleys beneath the Greenland ice sheet, Nature Geoscience, 7, 418, http://dx.doi.org/10.1038/ngeo2167, 2014.

Morlighem, M., Bondzio, J., Seroussi, H., Rignot, E., Larour, E., Humbert, A., and Rebuffi, S.: Modeling of Store Gletscher's calving dynamics, West Greenland, in response to ocean thermal forcing, Geophysical Research Letters, 43, 2659–2666, https://doi.org/10.1002/2016GL067695, http://dx.doi.org/10.1002/2016GL067695, 2016GL067695, 2016.

Nick, F., van der Veen, C., Vieli, A., and Benn, D.: A physically based calving model applied to marine outlet glaciers and implications for the glacier dynamics, Journal of Glaciology, 56, 781–794, https://doi.org/doi:10.3189/002214310794457344, http://www.ingentaconnect.com/content/igsoc/jog/2010/00000056/00000199/art00004, 2010.

Nye, J. F.: The Distribution of Stress and Velocity in Glaciers and Ice-Sheets, Proceedings of the Royal Society of London A: Mathematical, Physical and Engineering Sciences, 239, 113–133, https://doi.org/10.1098/rspa.1957.0026, http://rspa.royalsocietypublishing.org/content/239/1216/113, 1957.

Pollard, D., DeConto, R. M., and Alley, R. B.: Potential Antarctic Ice Sheet retreat driven by hydrofracturing and ice cliff failure, Earth and Planetary Science Letters, 412, 112 – 121, https://doi.org/http://dx.doi.org/10.1016/j.epsl.2014.12.035, http://www.sciencedirect.com/science/article/pii/S0012821X14007961, 2015.

Pralong, A. and Funk, M.: Dynamic damage model of crevasse opening and application to glacier calving, Journal of Geophysical Research (Solid Earth), 110, B01 309, https://doi.org/10.1029/2004JB003104, 2005.

Pralong, A., Funk, M., and Lüthi, M. P.: A description of crevasse formation using continuum damage mechanics, Annals of Glaciology, 37, 77–82, 2003.

Rignot, E. and Kanagaratnam, P.: Changes in the Velocity Structure of the Greenland Ice Sheet, Science, 311, 986–990, https://doi.org/10.1126/science.1121381, http://science.sciencemag.org/content/311/5763/986, 2006.

Rignot, E., Mouginot, J., Morlighem, M., Seroussi, H., and Scheuchl, B.: Widespread, rapid grounding line retreat of Pine Island, Thwaites, Smith, and Kohler glaciers, West Antarctica, from 1992 to 2011, Geophysical Research Letters, 41, 3502–3509, https://doi.org/10.1002/2014GL060140, http://dx.doi.org/10.1002/2014GL060140, 2014.

Ritz, C., Edwards, Tamsin L., Durand, Gaël, Payne, Antony J., Peyaud, Vincent, and Hindmarsh, Richard C. A.: Potential sea-level rise from Antarctic ice-sheet instability constrained by observations, Nature, 528, 115–118, https://doi.org/http://dx.doi.org/10.1038/nature16147 10.1038/nature16147, http://www.nature.com/nature/journal/v528/n7580/abs/nature16147.html#supplementary-information, 2015.

Schulson, E. M.: Brittle failure of ice, Engineering Fracture Mechanics, 68, 1839 – 1887, https://doi.org/http://dx.doi.org/10.1016/S0013-7944(01)00037-6, http://www.sciencedirect.com/science/article/pii/S0013794401000376, 2001.

Schulson, E. M., Iliescu, D., and Renshaw, C. E.: On the initiation of shear faults during brittle compressive failure: A new mechanism, Journal of Geophysical Research: Solid Earth, 104, 695–705, https://doi.org/10.1029/1998JB900017, http://dx.doi.org/10.1029/1998JB900017, 1999.

Shepherd, A., Ivins, E., Rignot, E., Smith, B., van den Broeke, M., Velicogna, I., Whitehouse, P., Briggs, K., Joughin, I., Krinner, G., Nowicki, S., Payne, T., Scambos, T., Schlegel, N., Geruo, A., Agosta, C., Ahlstrøm, A., Babonis, G., Barletta, V., Blazquez, A., Bonin, J., Csatho, B., Cullather, R., Felikson, D., Fettweis, X., Forsberg, R., Gallee, H., Gardner, A., Gilbert, L., Groh, A., Gunter, B., Hanna, E., Harig, C., Helm, V., Horvath, A., Horwath, M., Khan, S., Kjeldsen, K. K., Konrad, H., Langen, P., Lecavalier, B., Loomis, B., Luthcke, S., McMillan, M., Melini, D., Mernild, S., Mohajerani, Y., Moore, P., Mouginot, J., Moyano, G., Muir, A., Nagler, T., Nield, G., Nilsson, J., Noel, B., Otosaka, I., Pattle, M. E., Peltier, W. R., Pie, N., Rietbroek, R., Rott, H., Sandberg-Sørensen, L., Sasgen, I., Save, H., Scheuchl, B., Schrama, E., Schröder, L., Seo, K.-W., Simonsen, S., Slater, T., Spada, G., Sutterley, T., Talpe, M., Tarasov, L., van de Berg, W. J., van der Wal, W., van Wessem, M., Vishwakarma, B. D., Wiese, D., Wouters, B., and team, T. I. M. B. I. E.: Mass balance of the Antarctic Ice Sheet from 1992 to 2017, Nature, 558, 219–222, https://doi.org/10.1038/s41586-018-0179-y, 2018.

Slangen, A. B. A., Adloff, F., Jevrejeva, S., Leclercq, P. W., Marzeion, B., Wada, Y., and Winkelmann, R.: A Review of Recent Updates of Sea-Level Projections at Global and Regional Scales, pp. 395–416, Springer International Publishing, Cham, https://doi.org/10.1007/978-3-319-56490-6_17, https://doi.org/10.1007/978-3-319-56490-6_17, 2017.

Todd, J., Christoffersen, P., Zwinger, T., Råback, P., Chauché, N., Benn, D., Luckman, A., Ryan, J., Toberg, N., Slater, D., and Hubbard, A.: A Full-Stokes 3-D Calving Model Applied to a Large Greenlandic Glacier, Journal of Geophysical Research: Earth Surface, 123, 410–432, https://doi.org/10.1002/2017JF004349, https://agupubs.onlinelibrary.wiley.com/doi/abs/10.1002/2017JF004349, 2018.

van der Veen, C. J.: Fundamentals of Glacier Dynamics, A.A. Balkema, 1999.

van Der Veen, J.: Tidewater calving, Journal of Glaciology, 42, 375–385, https://doi.org/doi:10.3198/1996JoG42-141-375-385, http://www.ingentaconnect.com/content/igsoc/jog/1996/00000042/00000141/art00018, 1996.

Vieli, A., Jania, J., and Kolondra, L.: The retreat of a tidewater glacier: observations and model calculations on Hansbreen, Spitsbergen, Journal of Glaciology, 48, 592–600, https://doi.org/doi:10.3189/172756502781831089, http://www.ingentaconnect.com/content/igsoc/jog/2002/00000048/00000163/art00013, 2002.

Walter, F., O'Neel, S., McNamara, D., Pfeffer, W. T., Bassis, J. N., and Fricker, H. A.: Iceberg calving during transition from grounded to floating ice: Columbia Glacier, Alaska, Geophysical Research Letters, 37, n/a–n/a, https://doi.org/10.1029/2010GL043201, http://dx.doi.org/10.1029/2010GL043201, 2010.

WCRP Global Sea Level Budget Group: Global sea-level budget 1993–present, Earth System Science Data, 10, 1551–1590, https://doi.org/10.5194/essd-10-1551-2018, https://www.earth-syst-sci-data.net/10/1551/2018/, 2018.

Weertman, J.: Can a water-filled crevasse reach the bottom surface of a glacier, IASH Publ, 95, 139–145, 1973.

Weiss, J. and Schulson, E. M.: Coulombic faulting from the grain scale to the geophysical scale: lessons from ice, Journal of Physics D: Applied Physics, 42, 214 017, http://stacks.iop.org/0022-3727/42/i=21/a=214017, 2009.

Xie, S., Dixon, T. H., Voytenko, D., Deng, F., and Holland, D. M.: Grounding line migration through the calving season at Jakobshavn Isbræ, Greenland, observed with terrestrial radar interferometry, The Cryosphere, 12, 1387–1400, https://doi.org/10.5194/tc-12-1387-2018, https://www.the-cryosphere.net/12/1387/2018/, 2018.

Zhang, H., Ju, L., Gunzburger, M., Ringler, T., and Price, S.: Coupled Models and Parallel Simulations for Three-Dimensional Full-Stokes Ice Sheet Modeling, Numerical Mathematics: Theory, Methods and Applications, 4, 396–418, https://doi.org/10.1017/S1004897900000416, 2011.